CERN-TH/99-247
YITP-99-47
hep-ph/9908387

Isolated-photon production in polarized pp collisions

Stefano Frixione
CERN, TH Division, Geneva, Switzerland

Werner Vogelsang
C.N. Yang Institute for Theoretical Physics
State University of New York at Stony Brook
Stony Brook, NY 11794-3840, USA

Abstract

We perform a detailed study of the production of isolated prompt photons in polarized hadronic collisions, in the centre-of-mass energy range relevant to RHIC. We compare the results obtained for a traditional cone-isolation prescription, with those obtained by imposing an isolation condition that eliminates any contribution to the cross section from the fragmentation mechanism. The latter prescription will allow us to present the first fully consistent next-to-leading order calculation in polarized prompt-photon production. We will discuss the theoretical uncertainties affecting the cross section, addressing the issue of the reliability of the perturbative expansion, for both inclusive isolated-photon and photon-plus-jet observables. Finally, we will study the dependence of our predictions upon the polarized parton densities, and the implications for the measurability of the gluon density.

CERN-TH/99-247
August 1999

1 Introduction

A direct measurement of the gluon distribution in the proton is both very interesting and very difficult. This is true, in particular, for the spin-dependent gluon density Δg of a longitudinally polarized proton. So far, the only information on the nucleon polarized parton distributions comes from polarized deep-inelastic lepton–nucleon scattering (DIS). Here, in principle, Δg could be determined from scaling violations; however, in practice this procedure is afflicted by very large uncertainties due to the limited accuracy of the data and, in particular, to the fact that so far only *fixed-target* DIS experiments have been carried out in the polarized case, which, consequently, have a rather limited lever arm in Q^2. Thus, the proton spin-dependent gluon density Δg is experimentally constrained only very little so far.

In order to perform a direct determination of the gluon distribution, one needs to consider physical processes, which are predominantly initiated by gluons at the parton level; the contamination from quark-initiated subprocesses must be under good theoretical control; and finally, the process must take place at a measurable rate, taking experimental efficiencies into proper account. Only a few processes are known that meet all these requirements. One example is the production of heavy flavours in photon-hadron collisions; the cross section for this process in the case of polarized scattering has recently been computed [1] in QCD at next-to-leading order (NLO). The COMPASS collaboration at CERN [2], and possibly even HERA in the polarized configuration [3], will be able to exploit charm production in order to constrain the polarized gluon density. Such measurements are on the other hand severely limited by the low experimental efficiency of charmed-meson tagging.

A second possibility is given by jet hadro- and photoproduction; also in this case, QCD cross sections for polarized collisions are now known to NLO [4, 5]. It will indeed be attempted to determine Δg, at the forthcoming polarized RHIC pp collider [6], by a measurement of the spin asymmetry in jet production, and the recent study of ref. [4] has demonstrated that this approach has very promising prospects.

In the unpolarized case, the classical tool for determining the gluon density at intermediate and large x has been prompt-photon production, $pp \to \gamma X$ and $pN \to \gamma X$, in fixed-target experiments [7]. Indeed, data on prompt photons have been the backbone of the gluon determination in many analyses of parton densities. The main reason for this is that, at leading order, a photon in the final state is produced in the reactions $qg \to \gamma q$ and $q\bar{q} \to \gamma g$, with the contribution of the former subprocess being obviously sensitive to the gluon and usually dominant over that of the latter. It is the 'point-like' coupling of the photon to the quark in these subprocesses that is responsible for a much cleaner signal than, say, for the inclusive production of a π^0, which proceeds necessarily through a fragmentation process.

The cleanliness of the signal is of course an advantage that also counts at colliders. The aim of this paper is to provide a detailed study, performed in perturbative QCD at NLO accuracy, of the production mechanism for prompt photons at *polarized* hadronic colliders, such as RHIC. In the rest of this introduction, we will briefly review the present theoretical knowledge of prompt-photon production. In particular, we will explain why, in our opinion, a theoretical reappraisal of this matter is needed, before the data-taking will start at RHIC.

Prompt-photon data obtained at hadronic colliders have been used as a constraint for the unpolarized gluon density [7]. Thinking of the polarized case again, it is clear that the production of photons with polarized beams at RHIC is likely to be a very promising source

of information on Δg. We note that having pp reactions (as opposed to $p\bar{p}$ ones as hitherto in the unpolarized case) is also an advantage, since the competing LO subprocess $q\bar{q} \to \gamma g$ does not receive any contributions from valence–valence scattering here. Compared to jets, the prompt-photon reaction shows a larger spin asymmetry, even though of course the jet rate is much higher at a given p_T, resulting in smaller statistical errors. Eventually, both reactions, plus also charm production and π^0 production in polarized pp scattering, can be utilized to constrain Δg at RHIC, and it will be interesting to see how far the various channels will provide compatible pieces of information, and/or whether they will complement one another.

Unfortunately, the cleanliness of the prompt-photon signal alleged above is limited. As is well known, photons can also be produced through a fragmentation process, in which a parton, scattered or produced in a QCD reaction, fragments into a photon plus a number of hadrons. The problem with the fragmentation component in the prompt-photon reaction is twofold: first, it brings us back to the dependence on non-perturbative fragmentation functions, similar to the case of pion production addressed above, even though for prompt-photon production of course only a certain part of the total signal depends on the fragmentation functions. So far, the photon fragmentation functions are only insufficiently known; first information is emerging from the LEP experiments [8]. Secondly, *all* QCD partonic reactions contribute to the fragmentation component; thus the advantage of having a priori only one partonic reaction ($q\bar{q} \to \gamma g$) competing with the signal ($qg \to \gamma q$) is lost, even though some of the subprocesses relevant to the fragmentation part at the same time result from a gluon initial state.

Numerical studies [9, 10, 11, 12] for photon production in unpolarized collisions, based on predictions [9, 13, 14] for the photon fragmentation functions that turned out to be compatible with the sparse LEP data, demonstrate that the fragmentation component is not messing up things too much, even though it cannot be neglected in a careful study. In the fixed-target regime, it amounts to an effect of about 20%. At collider energies, it would easily make up for about half of the observed photons; however, here the situation is saved by the so-called 'isolation' cut, which is imposed on the photon signal in experiment. Isolation is an experimental necessity: in a hadronic environment the study of photons in the final state is complicated by the abundance of π^0's, eventually decaying into pairs of γ's. The isolation cut simply serves to improve the signal-to-noise ratio: if a given neighbourhood of the photon is free of energetic hadron tracks, the event is kept; it is rejected otherwise. In principle, there is a large freedom in the choice of specific isolation cuts, the only requirement being that they must strongly suppress the background $\pi^0 \to \gamma\gamma$, while keeping the signal at a measurable rate. Traditionally, isolation is realized by drawing a cone of fixed aperture in azimuthal angle–pseudorapidity space around the photon, and by restricting the hadronic transverse energy allowed in this cone to a certain fraction (of the order of less than 10%) of the photon transverse energy. In this way, it is clear that the fragmentation contribution, resulting from an essentially collinear process, will be diminished [15]. In actual numbers, it is not expected [10, 11] that it will remain responsible for more than 15–20% of the photon signal after isolation.

Studies of the backgrounds to prompt-photon production expected for RHIC have been reported in refs. [16, 17, 18], based on parton-shower Monte-Carlo event generators. It is anticipated [16, 17] that isolation cuts will also have to be applied in prompt-photon measurements at polarized RHIC. When working out theory predictions for the (un)polarized

cross sections and the resulting spin asymmetry, it is crucial that the calculation properly treats all effects mentioned so far, in particular those related to fragmentation and isolation.

It is the objective of this paper to do just this. Of course, it must be pointed out that several studies with a similar focus have been presented before. In particular, after the basic idea of determining Δg in $\vec{p}\vec{p} \to \gamma X$ had been formulated and developed in ref. [19], the QCD corrections to the 'direct' (i.e. *non*-fragmentation) component of polarized prompt-photon production were first calculated in refs. [20, 21] and applied for phenomenological predictions in refs. [22, 23]. There, the fragmentation component was neglected altogether, and no isolation cut was imposed. The calculations presented in refs. [20, 21] are fully analytical and can be used only for calculating the single-inclusive photon cross section, and not for looking at, say, photon-plus-jet final states. Still, it was demonstrated [24] how the effects of the isolation cut can be implemented into these calculations in the approximation that the isolation cone be rather narrow. Much more complete phenomenological studies were presented for the case of inclusive photons in ref. [25] and for $\vec{p}\vec{p} \to \gamma + jet + X$ in ref. [26]. In these papers, a Monte-Carlo code for the NLO corrections to the direct part of the cross section was developed and employed, which readily allows the isolation constraints to be taken into account. The results presented in refs. [25, 26] suffer from the fact that the fragmentation component to the polarized cross section could be treated at the LO level only, since the corresponding NLO corrections had not yet been calculated. This is potentially hazardous, since beyond LO the direct as well as the fragmentation part of the cross section depends on the factorization convention chosen in subtracting the final-state collinear singularities. Only their sum is free of scheme-dependence and is physical, which implies that a fully consistent NLO calculation affords knowledge of both production mechanisms at NLO, even though using a LO fragmentation contribution instead of the NLO one presumably introduces only a minor error from a numerical point of view. We emphasize that this situation has not improved since then, and it is not the purpose of this paper to do this. Still, this paper will present the first *fully consistent* NLO calculation of polarized prompt-photon production.

We believe that we have several good reasons for presenting a further phenomenological study on prompt photons at RHIC. First of all, our predictions will be based on the use of a new type of photon isolation constraint, introduced recently by one of us [27], which has the virtue of entirely eliminating the unwanted fragmentation component to the cross section. The basic idea of ref. [27] is not only to restrict the total hadronic energy falling into the isolation cone, but to allow less and less hadronic energy, the closer to the photon it is deposited, until eventually no energy at all is allowed exactly collinear to the photon. In this way, no collinear configuration is possible, and fragmentation does not contribute to the cross section. This feature allows us to present complete and theoretically consistent NLO predictions for polarized prompt-photon production. This will be done in terms of a dedicated Monte-Carlo program, which implements the new type of isolation in both polarized and unpolarized hadronic collisions. The isolation constraint we promote should be straightforwardly implementable in experiment. Here, we have in mind in particular the PHENIX detector at RHIC, with the very fine granularity of its electromagnetic calorimeter [16]; also the STAR detector [17], with its much larger angular coverage and its ability to see jets, appears to offer promising prospects.

Another motivation for our study is to look in more detail at the main theoretical uncertainties in the calculation, resulting from the scale dependence of the results. Furthermore,

previous theoretical studies have not really sufficiently addressed the question of the experimentally achievable statistical accuracy in the various conceivable measurements of the spin asymmetries in prompt-photon production. This will also be done in this paper. Here, we somewhat disagree with some previous conclusions concerning the usefulness of inclusive measurements compared with photon-plus-jet ones.

Presenting a study on prompt photons, we cannot ignore a disagreeable development found in the *un*polarized case in the last few years concerning the comparison between theory predictions and data. While things worked out very well in the first decade or so of prompt-photon experiments, the agreement with the more recent, and the most precise, data sets [28] is rather poor and sometimes so bad that the situation cannot possibly be saved even by 'fine'-tuning the unpolarized gluon density! Clearly, if this situation persists, we will have to worry about whether one can really interpret, in the polarized case, future RHIC data straightforwardly in terms of Δg. A possible remedy for this trend has been brought forward in terms of a smearing of the transverse momenta of the initial partons participating in the hard scattering [29, 30], required to be substantially larger than what is already introduced by the NLO calculation. This approach still remains to be set on a more solid foundation – eventually it should be accounted for to some extent by a k_T-resummation calculation [31] with perturbative as well as non-perturbative components. Furthermore, threshold resummations [32], aiming at the high-p_T end, have been shown [33] to lead to a certain improvement in the fixed-target regime. We also note that possible inconsistencies between the various data sets themselves have been pointed out [12]. It remains to be seen whether or not the agreement between data and theory will be in better shape by the time RHIC will perform the first measurements on $\vec{p}\vec{p} \to \gamma X$, as a result of the present experimental and, in particular, theoretical efforts in this field. Whatever the solution will eventually be, NLO theory, as employed in this work, will certainly be an indispensable part of it; it should then be straightforward to implement the lessons from the unpolarized case to the polarized one. It should not be forgotten either that RHIC itself should be able to provide new and complementary information also in the unpolarized case – never before have prompt-photon data been taken in pp collisions at energies as high as $\sqrt{S}$ =200–500 GeV.

The remainder of the paper is organized as follows. In section 2 we will provide the framework for our calculations. The new isolation definition will be presented in more detail, as well as the main ingredients for our Monte-Carlo code. The remaining sections are devoted to numerical studies for RHIC. Section 3 deals with the single-inclusive cross section. In subsection 3.1 we focus on issues related to perturbative stability, theoretical uncertainties and the effects of isolation. Subsection 3.2 is devoted to studies of spin asymmetries for the prompt-photon process at RHIC and of the sensitivity to Δg. In section 4 we consider more differential variables, such as photon-plus-jet ones. Here, subsection 4.1 discusses some general features of photon-plus-jet observables and also addresses their perturbative stability, while subsection 4.2 presents phenomenological results. Finally, we summarize our work in section 5.

2 Isolated photons in perturbative QCD

2.1 Isolation prescriptions

The production of isolated photons in hadronic collisions can be written in perturbative QCD as follows

$$
\begin{aligned}
&d\sigma_{AB}(K_A, K_B; K_\gamma) = \\
&\quad \int dx_1 dx_2 f_a^{(A)}(x_1, \mu_F) f_b^{(B)}(x_2, \mu_F) d\hat{\sigma}^{isol}_{ab,\gamma}(x_1 K_A, x_2 K_B; K_\gamma; \mu_R, \mu_F, \mu_\gamma) \\
&+ \int dx_1 dx_2 dz f_a^{(A)}(x_1, \mu'_F) f_b^{(B)}(x_2, \mu'_F) d\hat{\sigma}^{isol}_{ab,c}(x_1 K_A, x_2 K_B; K_\gamma/z; \mu'_R, \mu'_F, \mu_\gamma) D_\gamma^{(c)}(z, \mu_\gamma), \quad (1)
\end{aligned}
$$

where A and B are the incoming hadrons, with momenta K_A and K_B respectively, and a sum over the parton indices a, b and c is understood. In the first term on the RHS of eq. (1), denoted as the direct component, the subtracted (factorized) partonic cross sections $d\hat{\sigma}^{isol}_{ab,\gamma}$ get contributions from all the diagrams with a photon leg. On the other hand, the subtracted partonic cross sections $d\hat{\sigma}^{isol}_{ab,c}$ appearing in the second term on the RHS of eq. (1) (denoted as the fragmentation component), get contribution from the pure QCD diagrams, with one of the partons eventually fragmenting in a photon, in a way described by the (perturbatively uncalculable but universal) parton-to-photon fragmentation function $D_\gamma^{(c)}$. Equation (1) is to be regarded as a generic expression for the cross section: it will apply to unpolarized as well as polarized cross sections; in the latter case one simply has to substitute the parton densities $f_i^{(h)}$ and the partonic cross sections $d\hat{\sigma}^{isol}_{ab,r}$ with their spin-dependent counterparts, $\Delta f_i^{(h)}$ and $d\Delta\hat{\sigma}^{isol}_{ab,r}$ respectively. Note, however, that the parton-to-photon fragmentation functions $D_\gamma^{(c)}$ are always the unpolarized ones since we are not measuring the polarization of the produced photon.

As the notation in eq. (1) indicates, the isolation condition is embedded into the partonic cross sections. As mentioned in the introduction, for all the isolation conditions known at present, except that of ref. [27], as well as for the case of totally inclusive (non-isolated) photon production, neither the direct nor the fragmentation components are *separately* well defined at any fixed order in perturbation theory: only their sum is physically meaningful. In fact, the direct component is affected by quark-to-photon collinear divergences, which are subtracted by the bare fragmentation function that appears in the unsubtracted fragmentation component. Of course, this subtraction is arbitrary as far as finite terms are concerned. This is formally expressed in eq. (1) by the presence of the same scale μ_γ in both the direct and fragmentation components: a finite piece may be either included in the former or in the latter, without affecting the physical predictions. The need for introducing a fragmentation contribution is physically better motivated from the fact that a QCD hard scattering process may produce, again through a fragmentation process, a ρ meson that has the same quantum numbers as the photon and can thus convert into a photon, leading to the same signal.

Owing to the presence of the fragmentation remnants, which surround the emitted photon, the effect of the isolation cuts will be a stronger suppression of the fragmentation component relative to the direct component, with respect to the case of totally inclusive photon production. Since the parton-to-photon fragmentation functions are extremely poorly known, one may adopt two opposite points of view.

- Define the isolation cuts in order to suppress as much as possible the fragmentation component. The resulting cross section will be useful to measure the incoming gluon density or to test the predictions of the underlying theory. In this context, the unknown fragmentation functions are regarded as uncertainties affecting the theoretical predictions.

- Define the isolation cuts in order to keep a non-negligible contribution from the fragmentation component. The comparison between data and the resulting cross section will eventually be used to extract the parton-to-photon fragmentation functions. This strategy makes most sense if the initial state is as clean as possible, which is the case for e^+e^- collisions.

The former criterion leads to the so-called cone approach [15, 24, 34]. After tagging the photon, one draws a cone of half-angle R_0 around it. The word 'cone' can be misleading, being motivated by e^+e^- physics. Here, the cone is drawn in the pseudorapidity–azimuthal angle plane, and corresponds to the set of points

$$\mathcal{C}_{R_0} = \left\{ (\eta, \phi) \mid \sqrt{(\eta - \eta_\gamma)^2 + (\phi - \phi_\gamma)^2} \leq R_0 \right\}, \tag{2}$$

where η_γ and ϕ_γ are the pseudorapidity and azimuthal angle of the photon, respectively. The quantity in eq. (2) is boost-invariant, and is therefore suited to be used in collider physics. For the photon to be defined as isolated, the total amount of hadronic transverse energy $E_{T,had}(R_0)$ found in this cone must fulfil the following condition:

$$E_{T,had}(R_0) \leq \epsilon_c p_{T\gamma}, \tag{3}$$

where ϵ_c is a small number, and $p_{T\gamma}$ is the transverse momentum of the photon. This isolation prescription was proven to be infrared safe at all orders of perturbation theory in ref. [35]. The smaller ϵ_c, the tighter the isolation. Loosely speaking, for vanishing ϵ_c the direct component behaves like $\log \epsilon_c$, while the fragmentation component behaves like $\epsilon_c \log \epsilon_c$. Thus, for $\epsilon_c \to 0$ eq. (1) diverges. This is obvious since the limit $\epsilon_c \to 0$ corresponds to a fully-isolated cross section, which cannot be a meaningful quantity, whether experimentally (because of limited energy resolution) or theoretically (because there is no possibility for soft particles to be emitted into the cone).

On the other hand, if one actually wants to measure the fragmentation functions, then the so-called democratic approach should be adopted [36]. The basic idea here is to treat the photon as a QCD parton in a jet-clustering algorithm, and then to impose a cut on the hadronic energy contained in the 'jet', which also contains the photon. This approach has so far been used only in e^+e^- physics, and we will not discuss it any further in this paper.

In the spirit of the cone approach, an alternative definition of the isolated photon has been proposed [27]. After drawing a cone of half-angle R_0 around the photon axis, all the cones of half-angle $R \leq R_0$ are considered; their definition is identical to the one given in eq. (2), with R_0 replaced by R. Denoting by $E_{T,had}(R)$ the total amount of hadronic transverse energy found in each of these cones, the photon is isolated if the following inequality is satisfied:

$$E_{T,had}(R) \leq \epsilon_\gamma p_{T\gamma} \mathcal{Y}(R), \tag{4}$$

for *all* $R \leq R_0$. A sensible choice for the function $\mathcal{Y}$ is the following

$$\mathcal{Y}(R) = \left(\frac{1-\cos R}{1-\cos R_0}\right)^n, \qquad n = 1. \tag{5}$$

It has been proved in ref. [27] that such a choice allows the definition of an isolated-photon-plus-jet cross section, which is infrared-safe to all orders in QCD perturbation theory and still does not receive any contribution from the fragmentation mechanism. In this case, therefore, only the first term on the RHS of eq. (1) is different from zero, and it does not contain any μ_γ dependence. The reader can find all the technical details concerning the isolation prescription based on eq. (4) of ref. [27]. Here, we will just recall the main ideas. The fundamental property of the function $\mathcal{Y}$ is

$$\lim_{R\to 0} \mathcal{Y}(R) = 0, \tag{6}$$

the function being different from zero everywhere except for $R = 0$. This implies that the energy of a parton falling into the isolation cone $\mathcal{C}_{R_0}$ is correlated to its distance (in the η–ϕ plane) from the photon. In particular, a parton becoming collinear to the photon is also becoming soft. When a quark is collinear to the photon, there is a collinear divergence; however, if the quark is also soft, this divergence is damped by the quark vanishing energy (provided that the energy vanishes fast enough; this condition is not very restrictive, and the form in eq. (5) easily fulfils it). When a gluon is collinear to the photon, then either it is emitted from a quark, which is itself collinear to the photon – in which case, what was said previously applies – or the matrix element is finite. Finally, it is clear that the isolation condition given above does not destroy the cancellation of soft singularities, since a gluon with small enough energy can be emitted anywhere inside the isolation cone. The fact that this prescription is free of final-state QED collinear singularities implies that the direct part of the cross section is finite. As far as the fragmentation contribution is concerned, in QCD the fragmentation mechanism is purely collinear. Therefore, by imposing eq. (4), one forces the hadronic remnants collinear to the photon to have zero energy. This is equivalent to saying that the fragmentation variable z is restricted to the range $z = 1$. Since the parton-to-photon fragmentation functions do not contain any $\delta(1-z)$, this means that the fragmentation contribution to the cross section is zero, because an integration over a zero-measure set is carried out.

We stress that the function given in eq. (5) is to a very large extent arbitrary. Any sufficiently well-behaved function, fulfilling eq. (6), could do the job, the key point being the correlation between the distance of a parton from the photon and the parton energy, which must be strong enough to cancel the quark-to-photon collinear singularity. We also remark that the traditional cone-isolation prescription, eq. (3), can be recovered from eq. (4) by setting $\mathcal{Y} = 1$ and $\epsilon_\gamma = \epsilon_c$. In the rest of this paper, as a short-hand notation, we will indicate the 'traditional' isolation obtained by imposing eq. (3) as **definition A**, and that obtained by imposing eq. (4) as **definition B**.

At first sight, the new isolation approach appears to be stricter than the traditional one. On the other hand, the fact that for the new constraint one also considers the angle between the photon and hadrons in the cone, is a real virtue here: for the traditional criterion, one would reject a hadron of, say, 2 GeV wherever it is located in the cone, just because its energy exceeds the limit. Of course, if the cone size is 0.7, and the hadron has a distance of

0.6 with respect to the photon – why should one want to reject such an event? This situation is improved with the new constraint: hadrons in the cone that are still quite far away from the photon are allowed to have more energy than those close to the photon. In this way, one can well allow a hadron to have 2 GeV, or even more, at a distance of 0.6. This little example implies that a detailed comparison between the traditional and the new isolation methods is certainly of some interest, and this will also be performed in this paper. One can then eventually decide which isolation to use in actual experiment.

2.2 NLO computer codes

In order to give phenomenological predictions, we will use two different computer codes in the cases of definitions A and B. As far as definition A is concerned, we use the NLO program of refs. [21, 24] for the direct part of the cross section. This program is based on an inclusive calculation of the contributing partonic subprocesses $ab \to \gamma X$ to NLO, where X contains a sum over the appropriate partonic final states, fully integrated over their phase spaces. The advantage of this approach is that all contributions to a given partonic channel, such as virtual and real-emission ones, and collinear counterterms, can be added before any numerical implementation. In this way, not only all singularities that appear in the calculation cancel, but there is no need to introduce any soft or collinear cut-off at intermediate stages of the numerical calculation either. One therefore ends up with a rather fast and accurate code. However, the drawback of this is the inclusiveness of the program: there is no handle on, say, an extra jet since the partons in the final state have been integrated over. As it stands, it would even seem impossible to implement isolation in such a code since this clearly affords to have control over partons falling into the isolation cone. However, as was shown in ref. [24], one can fairly straightforwardly make up for this latter deficit, provided the opening of the isolation cone is not too big. The idea is as follows: at NLO, the isolated cross section can also be viewed as the *non*-isolated one *minus* the cross section for a parton to be in the cone, having more energy than that allowed by the isolation cut. This latter 'subtraction' cross section can be approximated in a fairly simple calculation in the limit of a narrow isolation cone, since it is dominated by almost collinear quark–photon configurations. As a result, the 'subtraction' piece turns out to behave like $\mathcal{A} \ln R_0 + \mathcal{B} + \mathcal{O}(R_0^2)$; $\mathcal{A}, \mathcal{B}$ are presented in [24] for both the unpolarized and the polarized cases. Note that the 'subtraction' piece itself inevitably depends on the final-state factorization scale μ_γ introduced in eq. (1).

As we discussed in the previous subsection, for definition A the fragmentation mechanism contributes (cf. eq. (1)). We also stated in the introduction that in the polarized case we presently cannot calculate this part at NLO and thus have to stick to a LO calculation for it. In contrast to this, in the *un*polarized case the NLO corrections to the relevant partonic scatterings are known [37]. The calculation and computer code presented in ref. [37] were also fully inclusive in the sense that the unobserved partons had been integrated over their full phase spaces. However, as was shown in ref. [24], the above 'narrow-cone' approximation can also be used to implement isolation in the NLO fragmentation component as calculated with the program of ref. [37]. When calculating the unpolarized prompt-photon cross section for definition A in this paper (for the purpose of computing asymmetries), we will always include the fragmentation part at NLO, making use of the program of ref. [37], along with the modifications for isolation developed in ref. [24].

The code relevant to definition B works in a completely different way, being fully exclusive in the variables of the photon and of the (one or two) final-state QCD partons. It is based on the formalism presented in refs. [38, 39], which allows the computation of any infrared-safe observables for any kind of scattering particles, without requiring algebraic manipulations on the matrix elements. The formalism adopts the subtraction method in order to deal with soft and collinear singularities, and therefore both the matrix elements and the phase space are treated without any approximation. The code used in this paper is an extension of that presented in ref. [40], which deals with the production of isolated photons in *un*polarized hadronic collisions. Notice that the formalism of refs. [38, 39], although originally designed for the case of unpolarized collisions, extends – basically without any modifications – to the case of polarized collisions. A detailed discussion on this topic can be found in ref. [4]. We finally mention the fact that the code outputs the kinematical variables of the photon and of the final-state partons, plus a suitable weight. Therefore, the isolation condition, the jet-reconstruction algorithm, and any cuts matching the experimental setup can be implemented as the final step of the computation algorithm. This allows us to plot as many observables as we want in one single computer run.

It is easy to see that one can extend the ideas behind the 'narrow-cone' approximation, used for the definition-A code, also to the isolation given by definition B. In this way, we have been able to compare extensively the results of the two codes. We found excellent agreement of the two programs over a wide range of kinematical variables, and also for cone openings of even $R_0 = 0.7$, if only central values of rapidity are considered. This suggests the correctness of the two – entirely independent – codes. It also implies that the 'narrow-cone' approximation has a rather large region of validity and can be well used for practical applications. We recall, however, that the corresponding code is only suitable for fully-inclusive photon observables, and not for photon-plus-jet ones.

3 Inclusive isolated-photon observables

In this section, we study the inclusive properties of isolated photons. More exclusive observables, such as correlations between the photon and the accompanying jets, will be discussed in section 4. We will consider centre-of-mass energies spanning the range $\sqrt{S}$ =200–500 GeV. We will carefully investigate the differences induced by the different isolation prescriptions we deal with in this paper. We will address the issue of the perturbative stability of our results, and study the dependence of the cross sections upon the polarized parton densities.

3.1 Effects of isolation and discussion of theoretical uncertainties

Unless otherwise specified, we will use the following parameters, as a default for our calculations:

$$R_0 = 0.4, \quad \epsilon_c = \frac{1 \text{ GeV}}{p_{T\gamma}}, \qquad \text{definition A;} \tag{7}$$

$$R_0 = 0.4, \quad \epsilon_\gamma = 1, \quad n = 1, \qquad \text{definition B.} \tag{8}$$

It is worth emphasizing at this point that we have chosen $\epsilon_\gamma \gg \epsilon_c$: for traditional isolation A, ϵ_c has to be small – otherwise, isolation is totally ineffective. For isolation B, on the other

hand, ϵ_γ may be chosen large, as we discussed previously. A large ϵ_γ only means that one still allows considerable amounts of hadronic energy in the cone, provided it is deposited far away from the photon. We add that it is actually desirable theoretically in any isolation to have a 'large' value of ϵ ($= \epsilon_\gamma$ or ϵ_c): soft-gluon emission into the cone generates logarithms [15, 24, 27] of ϵ, with an extra power at each further order of perturbation theory, which for very small ϵ eventually threaten to spoil the perturbative expansion. A study on the structure of the logarithms appearing in the isolated-photon cross section in e^+e^- collisions has been given in ref. [35]. Pending a more thorough investigation of these points in the case of isolation B, it seems likely that being able to choose $\epsilon_\gamma = \mathcal{O}(1)$ is clearly a virtue of this isolation method.

The default value for the factorization and renormalization scales will be indicated by μ_0, which will be taken equal to the transverse momentum of the photon in the case A, and equal to half of the total transverse energy of the event in the case B. These two choices, which slightly differ beyond LO, are due to the different structure of the codes computing the isolated-photon cross section in cases A and B, as described in section 2. It would be possible to set $\mu_0 = p_{T\gamma}$ in case B (however, this choice, although formally correct, is less appropriate than the one adopted here: since the code is fully exclusive in the variables of the photon and of the final-state partons, the reference scale, which is directly related to the hardness of the process, should also depend upon the transverse momenta of the partons); this would result in differences with our default choice that are completely negligible when compared to the other sources of theoretical uncertainty affecting the cross section. We will adopt throughout the two-loop expression for α_s, the Λ_{QCD} value being that associated with the parton densities used. Our default parton density sets will be the NLO 'standard' set of ref. [41] (GRSV STD) and MRST [30] for the polarized and unpolarized scattering respectively. In the case of the definition A, we will use the NLO GRV [13] set of parton-to-photon fragmentation functions.

We have to note here that, while the value of Λ_{QCD} associated with the MRST set ($\Lambda_5^{\overline{\rm MS}} = 220$ MeV) is close to the central value of the latest PDG world average (at two loops, $\Lambda_5^{\overline{\rm MS}} = 237^{+26}_{-24}$ MeV [42]), all the available polarized density sets have a value which is much lower, consistent with that extracted from DIS data some years ago. Thus, by adopting the value of Λ_{QCD} associated with a given set, we have the unpleasant situation in which, in the computation of asymmetries, the numerator and the denominator have different Λ's. Still, we preferred not to violate the correlation between the parton densities and Λ_{QCD}. This correlation is expected to be particularly strong in the case of the gluon density, which is of great importance here. Since a smaller Λ_{QCD} entails a smaller strong coupling, our predictions for asymmetries would have become somewhat larger than the ones we present below, had we decided to adopt the same value of Λ_{QCD} in the polarized and unpolarized cross sections. This situation has already been encountered in ref. [4], for jet physics. There, it has been shown that using the same Λ_{QCD} in the polarized and unpolarized cross sections would increase the asymmetry by 15% (relatively) at the most. In the case of photon production, the difference is even smaller. As we will see, the effect is therefore completely negligible, with respect to the differences in the predictions of the asymmetries induced by the choice of different parton densities.

In what follows, in order to assess the importance of the radiative QCD corrections, we will often compare the NLO and Born results. Throughout the paper, by 'Born result' we will mean the prediction obtained by convoluting the lowest-order partonic cross sections ($\mathcal{O}(\alpha_{\rm em}\alpha_s)$ and $\mathcal{O}(\alpha_s^2)$ for the direct and the fragmentation contributions respectively) with

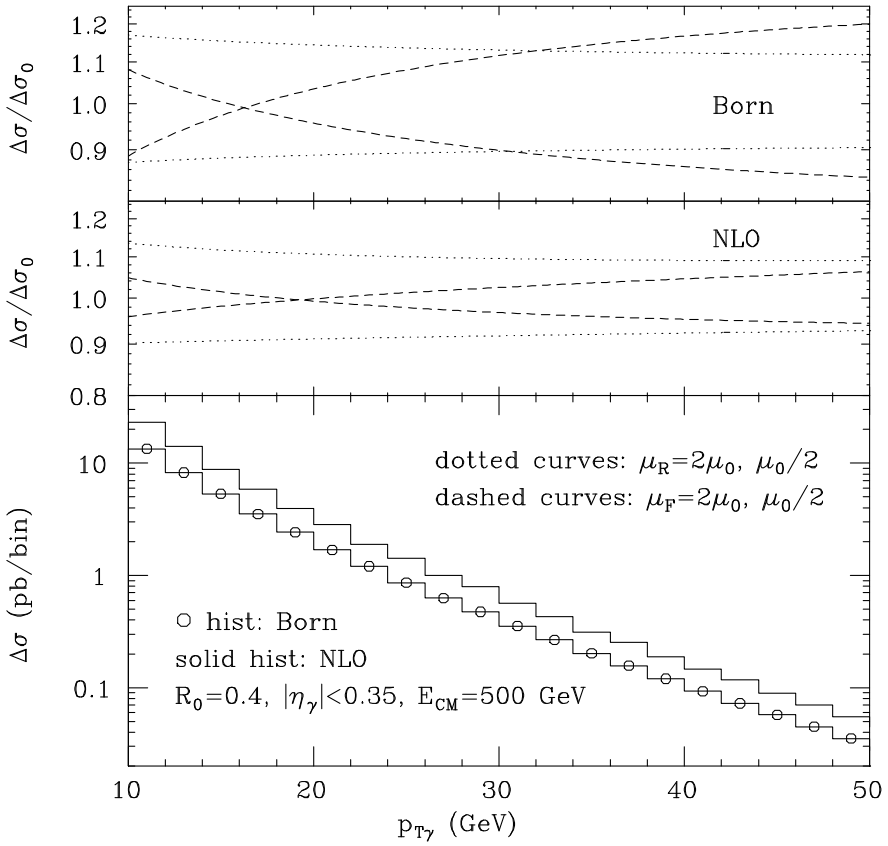

Figure 1: *Transverse-momentum spectrum of the isolated photon, in the case of definition B, for polarized pp collisions at $\sqrt{S}$ = 500 GeV. The polarized parton densities used are GRSV STD. The scale dependences of the Born and NLO results are also shown; see the text for details.*

the NLO-evolved parton densities and, if needed, fragmentation functions. Also, the two-loop expression of α_S will be used. There is of course a lot of freedom in the definition of a Born-level result. However, we believe that with this definition one has a better understanding of some issues related to the stability of the perturbative series. This is especially true in polarized physics, where the data are not sufficient to determine the parton densities with a good accuracy, and where large (artificial) differences can arise between sets fitted at LO or NLO to the available DIS data. For a detailed discussion on this point, see for example ref. [4].

We start by considering the transverse momentum spectrum of isolated photons. In the lower part of fig. 1 we plot the Born (histogram with symbols) and NLO (solid histogram) results for the polarized cross section, obtained at $\sqrt{S} = 500$ GeV with the isolation definition B. A cut $|\eta_\gamma| < 0.35$ has been imposed, which is suitable for the PHENIX experiment. As can be seen from the figure, the inclusion of the radiative corrections gives a sizeable effect as far as the normalization is concerned (in the first bin, the ratio of NLO over Born result is about 1.8), while the shape is almost unaffected (the Born being only slightly harder than

the NLO result). Since the radiative corrections are large, one may wonder whether the NLO result is a sensible quantity to compare with data. A rigorous answer to this question can only come from a complete NNLO calculation. Lacking that, we study the scale dependence of our results, as customary in perturbative QCD, to see whether the inclusion of radiative corrections leads to a milder dependence upon the scales, as compared to the one of the Born result. Here, it is especially important to study the separate dependence upon the renormalization and factorization scales, because cancellation effects between the two may hide some problems. We present the scale dependence of the $p_{T\gamma}$ spectrum in the upper and central parts of fig. 1. There, we show the ratio of the cross section obtained by setting the scales equal to $\mu_0/2$ and $2\mu_0$, over the cross section for the default values of the scales. We stress that only one scale is varied at a time. The renormalization (factorization) scale variation corresponds to the dotted (dashed) curves; the curves decreasing for increasing $p_{T\gamma}$ correspond to $\mu_R = \mu_0/2$ and $\mu_F = 2\mu_0$, respectively. From the figure, it is apparent that the inclusion of the radiative corrections reduces the scale dependence in the whole $p_{T\gamma}$ range considered, with a possible exception in the case of the μ_F dependence, for $p_{T\gamma}$ equal to 16–20 GeV, where there is basically no μ_F dependence. The reduction is stronger in the case of μ_F dependence than in the case of μ_R dependence. The fact that there is a point in the $p_{T\gamma}$ spectrum where there appears to be no factorization scale dependence is purely accidental; it can be traced back to the behaviour of the parton densities with respect to the hard scale. In fact, the gluon density increases with the scale in the x range corresponding to the low-$p_{T\gamma}$ region, while it is decreasing when the scale is increasing for larger x values, probed when a harder photon is produced. We can conclude from fig. 1 that the perturbative expansion seems to be reliable in this case; in all cases, the radiative corrections reduce the size of the dependence of the $p_{T\gamma}$ spectrum upon the scales. We must comment on the fact that this conclusion is not specific to the kinematical configuration considered in fig. 1: we verified that the same kind of behaviour can be seen in a larger η_γ range (we studied the case $-1 < \eta_\gamma < 2$), and also at lower centre-of-mass energies ($\sqrt{S} = 200$ GeV). Furthermore, almost the same results are obtained in the case of unpolarized collisions.

We now turn to the case when the photon is isolated according to definition A. The results are presented in fig. 2. In the lower part, we display the ratio of the cross section over that obtained with definition B. In this case, the scales are fixed to their default values. The result at the Born level is again displayed as a histogram with symbols. The Born result in the case of definition A is always higher than that relevant to definition B. This is easy to understand, since at this order the result for the direct part is independent of the isolation condition, and the photon isolated with definition A gets a contribution from the fragmentation part, which is not present in the case of definition B. Things of course change at NLO: having an additional parton around, the isolation condition is effective also in the direct part. We must also remark that, in the case of isolation A, the fragmentation contribution is only included at LO. A consistent computation at NLO would presumably produce a slightly larger cross section (for example, in the case of unpolarized collisions, the inclusion of radiative corrections in the fragmentation component enhances the full cross section at high p_T by about 3%). The effect is much larger in the case in which there is no isolation condition, and the photon is fully inclusive. We will further comment on this fact below. As in the previous case, we also studied the μ_R and μ_F dependence of the spectrum; in doing so, the factorization and renormalization scales of the direct and of the fragmentation components have been set to the same value:

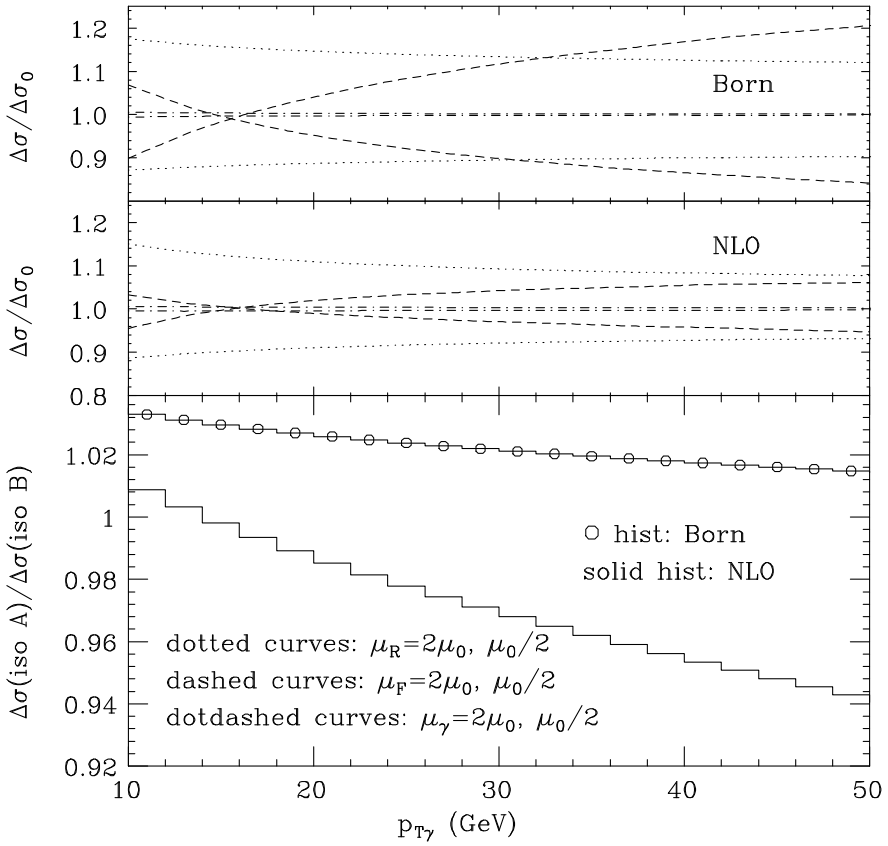

Figure 2: *Transverse-momentum spectrum of the isolated photon, in the case of definition A. The ratio of the cross section over that obtained with definition B is shown in the lower part. The rest of the figure displays the scale dependence, at the Born and NLO levels.*

$\mu'_F = \mu_F$ and $\mu'_R = \mu_R$ (see eq. (1)). The results are displayed in the upper parts of fig. 2. Note that for definition A we have an additional pair of lines (dot-dashed), corresponding to the results obtained by varying the *final*-state factorization scale μ_γ, which enters the fragmentation functions. The μ_F and μ_R dependence is very similar to the one relevant to definition B, displayed in fig. 1, and the same comments made previously apply here. On the other hand, the μ_γ dependence is extremely small, and gives a negligible contribution to the theoretical error affecting the cross section. The almost identical scale dependence in the case of definitions A and B also implies that the ratio of cross sections plotted in the lower part of fig. 1 is, to a good extent, independent of the scale choice.

For completeness, we present in fig. 3 the corresponding predictions for the fully inclusive *non-isolated* prompt-photon cross section. We first discuss the scale dependence of the results, displayed again in the upper two parts of the figure. At low $p_{T\gamma}$, the μ_R dependence turns out to be larger than that of the isolated-photon cross sections, while at large $p_{T\gamma}$ the two appear to be pretty similar (the isolation condition is less and less restrictive as the transverse momentum of the photon is increased, since it is more and more difficult to have a hard parton,

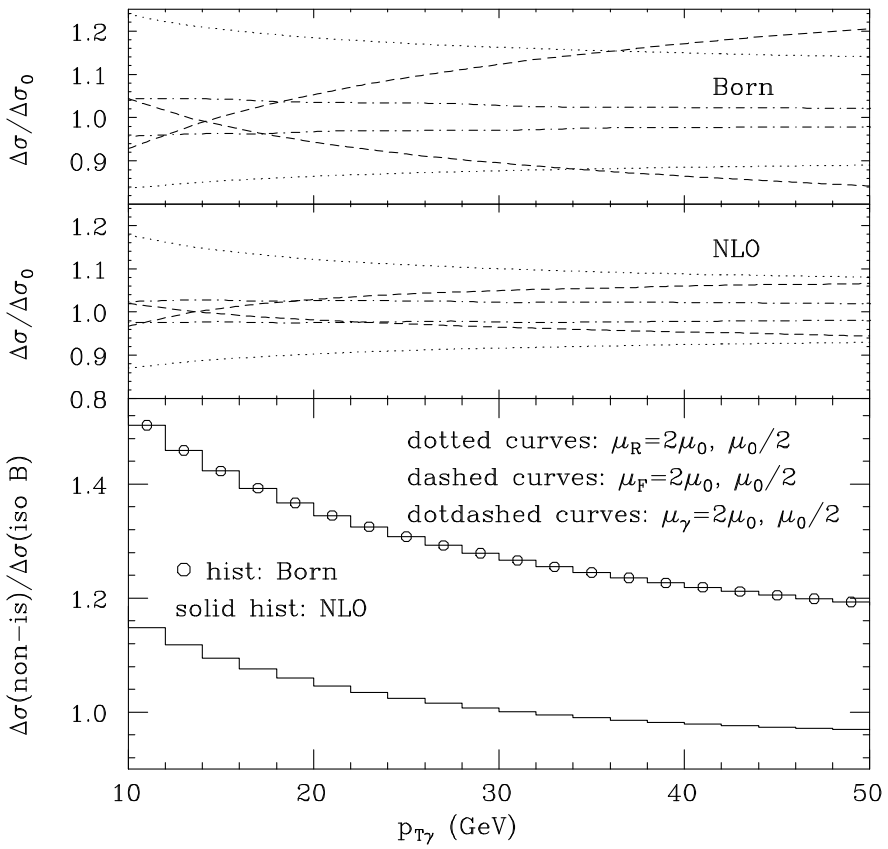

Figure 3: *Same as in fig. 2, for non-isolated photons.*

in the surroundings of the photon, that does not pass the isolation cuts). The μ_γ dependence of the fully inclusive cross section is much larger than that of the isolated-photon cross section obtained with definition A. However, its effect is still smaller than that due to μ_R and μ_F.

The comparison of the non-isolated cross section with the one isolated according to definition B is shown in the lower part of fig. 3. One immediately notices a striking feature: at NLO, the isolated cross section becomes larger than the unpolarized one at large $p_{T\gamma}$. Clearly, this finding is at odds with the physical expectation that any meaningful isolation cut should reduce the number of events with respect to the number obtained for no isolation at all. The origin of the problem we encounter resides in the fact that the fragmentation contribution to the non-isolated cross section (and, obviously, also for the results for isolation A presented in fig. 2) has only been calculated at the LO level since, as we pointed out earlier, the NLO corrections to the fragmentation contribution have not been calculated so far in the polarized case. We expect that once the proper NLO fragmentation component is included in the calculation of the polarized cross section, the disagreeable feature of fig. 3 will disappear. This view is corroborated by the observation that we find exactly the same pattern in the unpolarized case: there, everything can be calculated consistently at NLO, and the non-isolated cross section turns out to be larger than the one obtained for both types of isolation we consider. However, we checked that, *if* we compute the fragmentation contribution only at LO

in the unpolarized case, we indeed obtain a non-isolated cross section that is *smaller* than the isolated one for definition B, much as happens in fig. 3. The figure clearly points out the importance of consistency in the NLO calculation. A NLO calculation of the fragmentation component of the polarized prompt-photon cross section is highly desirable for the future. On the basis of fig. 3 we would predict non-negligible positive corrections to the LO result. For the time being, our present results for isolation A and the non-isolated case have only limited reliability. Fortunately, fragmentation is really important only in the non-isolated case, which is not the one relevant to experiment. For a (traditionally) isolated cross section, it contributes a relatively small fraction of the full result, and this fraction decreases rapidly towards larger $p_{T\gamma}$. We are therefore fairly confident that our predictions for definition A are numerically not too far off the true NLO answer.

For these reasons, we refrain from performing a detailed study of the uncertainty in the cross section for isolation A. We only state that we have also calculated the unpolarized and the polarized cross sections, using set I of the photon fragmentation functions of ref. [14]. We find that the fragmentation component to the cross section decreases by about 23% at $p_{T\gamma} \approx 10$ GeV, and by about 50% at the high-$p_{T\gamma}$ end. For the full (i.e. direct plus fragmentation) cross section, the effect is obviously much smaller, generally below 2%.

There is another striking property of the curve in the lower part of fig. 2: it is *very* close to unity over the whole range of $p_{T\gamma}$ (in fact, from what we just discussed, we would expect it to be even closer to unity at large $p_{T\gamma}$, had we been able to include the fragmentation component at NLO in case of definition A). In other words, the two types of isolation, albeit so different from a physics point of view, lead to almost identical cross sections. To some extent, this is certainly due to the choices we made for ϵ_c, ϵ_γ in eqs. (7),(8): had we chosen, say, $\epsilon_\gamma = \epsilon_c$ there[1], then isolation B would have become stricter than isolation A, and the corresponding curve in fig. 2 would have been above unity everywhere. Our choices in eqs. (7),(8) presumably created a certain 'balance' between the two isolations. However, we found that there is more to the similarity of the two isolated cross sections. When performing runs at larger values of R_0, we found that the cone-size dependence of the cross section is extremely mild for both types of isolation. This indicates that isolation is most effective close to the photon and does not affect the cross section too much at larger distances from the photon. To illustrate this point, we plot in fig. 4, as a function of the distance R from the photon, the amount of hadronic transverse energy deposited on average in a cone annulus between $R - \Delta R$ and $R + \Delta R$, where $\Delta R = 0.025$. We do this for isolation of type B, considering two realistic values of the isolation-cone size, $R_0 = 0.4$ and $R_0 = 0.7$, and one extreme value $R_0 = 0.005$. We have chosen $\sqrt{S} = 500$ GeV, and the photon variables have been integrated over $p_{T\gamma} > 10$ GeV, $-1 < \eta_\gamma < 2$ (we used an extended rapidity coverage in order to reduce as much as possible the statistical errors on our results; however, rapidity is not an issue here, and our conclusions apply to any rapidity range). The reason for having a plot obtained with $R_0 = 0.005$ is the following: with such a narrow isolation cone, the distribution in hadronic transverse energy around the photon is basically identical (for non-zero R) to what would be obtained in the case of non-isolated photons. Thus, we can have a clear idea of the effect of imposing an isolation condition with a realistic value for R_0. By inspection of the solid

[1]This is simply an example; as discussed at the beginning of this subsection, this is actually not a desirable choice.

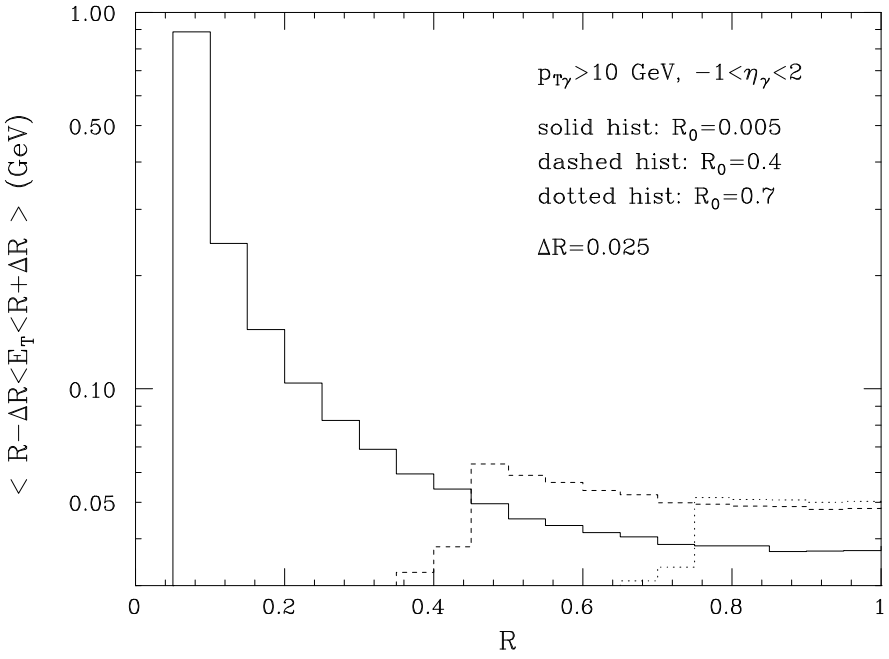

Figure 4: *Average transverse energy in the cone annuli around the photon.*

histogram in fig. 4, we see that a sizeable amount of energy is deposited only at small distances from the photon, and – at least in the framework of a NLO calculation – not much energy is delivered for $R >$0.2–0.3. This is the reason why there is no real difference between the cross sections obtained with different, but physically sensible, values of R_0. Notice that this conclusion holds regardless of whether we use isolation A or B. To avoid misunderstandings concerning fig. 4: of course at NLO we have only one extra particle at our disposal (the third one balancing the other two in transverse momentum), so isolation only becomes effective if this particle falls into the isolation cone. We are not saying in fig. 4 that this extra particle is usually soft: the point is rather that, thanks to the collinear singularity of the corresponding $2 \to 3$ matrix elements at $R = 0$, the extra particle simply happens to be close to the photon more often than far away from it, so that *on average* more energy is deposited close to the photon. Incidentally, one can convince oneself that, for small R and $\Delta R \ll R$, the quantity shown in fig. 4 has to be proportional to $\Delta R/\sigma(R_0) \times (d\sigma(\theta)/d\theta)_{\theta=R}$, where θ is the angle between the momenta of the photon and the other particle in the cone, and $\sigma(R_0)$ is the total cross section for a given isolation-cone size R_0 and a given kinematical range for the photon variables (here, $p_{T\gamma} > 10$ GeV and $-1 < \eta_\gamma < 2$). For a quark parallel to the photon (which is the only configuration producing a collinear singularity at $\theta = 0$), one thus finds immediately that the curves in fig. 4 should fall $\propto 1/R$ if $R > R_0$, i.e. outside the isolation cone. This is exactly the pattern observed in the figure. Inside the cone the isolation is effective, and for the isolation of definition B employed here, one expects the curve to fall like some power of R as $R \to 0$. Finally, we also note that the normalization factor $1/\sigma(R_0)$ is the reason why the histograms for the three different R_0 in fig. 4 do not exactly coincide even if $R > 0.7$. A comparison of the histograms relevant to $R_0 = 0.4$ and $R_0 = 0.7$ at $R = 1$ nicely demonstrates

how weak the dependence of the isolated-photon cross section on the cone size is.

We finally study the distribution of the photon in pseudorapidity η_γ. We impose here the

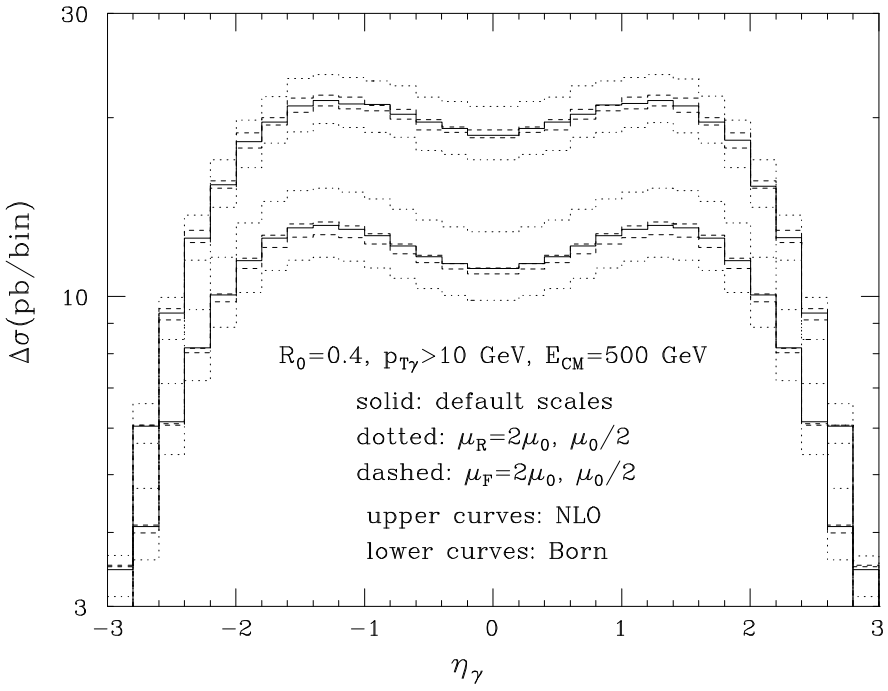

Figure 5: *Pseudorapidity spectrum of isolated photons (definition B). The cross sections obtained by varying the renormalization and factorization scales are also shown.*

transverse momentum cut $p_{T\gamma} > 10$ GeV. Our results are summarized in fig. 5; they have been obtained in the case of definition B. The upper histograms correspond to NLO, while the lower ones represent the Born level results. The solid histograms have been obtained with default scales. They are pretty similar in shape; the Born is only slightly broader, with a deeper dip at $\eta_\gamma = 0$. The size of radiative corrections is as expected from what we previously found for the $p_{T\gamma}$ spectrum: the NLO result is about a factor 1.6 higher than the Born one. The pairs of dotted histograms are obtained by setting the renormalization scale equal to $\mu_0/2$ and $2\mu_0$. It is clear that also in this case the radiative corrections have the effect of reducing the scale dependence; by varying μ_R, one obtains NLO cross sections that differ from the default one by 10% at most. The effect of varying the factorization scale is much smaller than that associated with changes in μ_R. This can be understood by looking at fig. 1: the effects at low $p_{T\gamma}$ ($\mu_F = \mu_0/2$ returns a cross section smaller than the default one) and at large $p_{T\gamma}$ ($\mu_F = \mu_0/2$ returns a cross section larger than the default one) tend to compensate when integrating over $p_{T\gamma}$, as done for fig. 5. The scale dependence of the densities is again responsible for this behaviour. When plotting the η_γ distribution for an integration over, say, just the region $10 < p_{T\gamma} < 12$ GeV, one would see a much larger μ_F dependence, of the order of that shown in the low-$p_{T\gamma}$ region in fig. 1. We also considered the η_γ spectrum in the case when the photon is isolated according to definition A. The scale dependence, as already in

the case of the $p_{T\gamma}$ spectrum, is identical to that presented in fig. 5. The shape is almost the same as the one relevant to definition B, for all scale choices.

3.2 Spin asymmetries and sensitivity to Δg

In spin physics, experiments usually focus on spin asymmetries, since many systematic uncertainties cancel out in this ratio of polarized and unpolarized cross sections. In what follows, we will therefore study the quantity

$$\mathcal{A}_{p_{T\gamma}} = \frac{d\Delta\sigma/dp_{T\gamma}}{d\sigma/dp_{T\gamma}}, \tag{9}$$

as a function of $p_{T\gamma}$. We will also consider a similar asymmetry, with $p_{T\gamma}$ replaced by η_γ. More studies on asymmetries will be presented in section 4. In eq. (9), it is understood that the same kinematical cuts are applied to both the numerator and the denominator. The measurability of a spin asymmetry for a given process, as far as statistics are concerned, is of course determined by the counting rate. The quantity

$$\left(\mathcal{A}_{p_{T\gamma}}\right)_{min} = \frac{1}{P^2}\frac{1}{\sqrt{2\sigma\mathcal{L}\epsilon}} \tag{10}$$

can be regarded as the minimal asymmetry that can be detected experimentally or, equivalently, as the expected statistical error of the measurement, for a given integrated luminosity relevant to parallel or antiparallel spins of the incoming particles, $\mathcal{L}$, beam polarizations P and a detection efficiency $\epsilon \leq 1$; σ is the unpolarized cross section integrated over a certain range in $p_{T\gamma}$ (this range is denoted as a $p_{T\gamma}$ bin). We assumed here that the luminosities relevant to parallel and antiparallel spins of the incoming protons are equal, $\mathcal{L}^{\rightrightarrows} = \mathcal{L}^{\rightleftarrows} \equiv \mathcal{L}$. If this were not the case, the quantity $2\sigma\mathcal{L}$ in eq. (10) would have to be substituted with $4\sigma\mathcal{L}^{\rightrightarrows}\mathcal{L}^{\rightleftarrows}/(\mathcal{L}^{\rightrightarrows} + \mathcal{L}^{\rightleftarrows})$.

At present, the largest source of uncertainty on the theoretical predictions for asymmetries is clearly the choice of the polarized parton densities. We established in the previous subsection that the perturbative expansion of single-inclusive cross sections is under control. In the remainder of this section, we will therefore concentrate on the dependence of the asymmetries upon the densities. There are many NLO-evolved sets available, which mainly differ in the gluon sector, which is rather poorly constrained by DIS data (apart, perhaps, from the first moment). In a previous study relevant to jet physics [4], we saw that most of the sets give almost identical results as far as the shape of the asymmetry is concerned, the main difference being in the absolute normalization. For this reason, we will limit ourselves in this paper to three sets: GRSV STD, our default set; GRSV MAXg [41], which has a much larger gluon density and is thus expected to return the highest cross sections; and set C of ref. [43] (GS-C), which has a rather small gluon density whose shape is dramatically different from that of all the other sets, turning negative at high x for Q^2 not too large.

In fig. 6 we present our results for the asymmetry as a function of $p_{T\gamma}$. A cut $|\eta_\gamma| < 0.35$ has been applied. In the left part of the figure we plot the asymmetries obtained at $\sqrt{S} = 200$ GeV, while in the right part we present the results for $\sqrt{S} = 500$ GeV. The solid, dashed and dotted histograms correspond to the NLO predictions obtained with GRSV STD, GRSV MAXg and

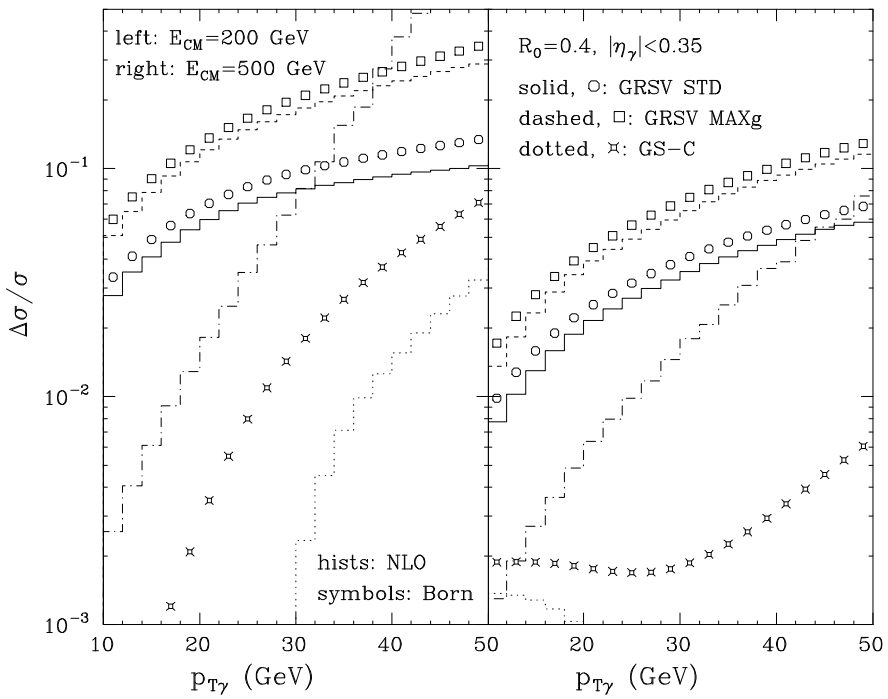

Figure 6: *Asymmetry as a function of $p_{T\gamma}$, for various polarized densities, at different centre-of-mass energies. The minimally observable asymmetry (dot-dashed histogram) is also shown.*

GS-C respectively. The corresponding symbols (see the labels on the figure) are the results obtained at the Born level. Finally, the dot-dashed histogram is the minimally observable asymmetry, as defined in eq. (10). We have chosen $\mathcal{L} = 100$ pb^{-1}, $P = 1$ and $\epsilon = 1$. Of course, the latter two choices are not realistic; however, in adopting this 'ideal-world' situation, we can estimate the optimally achievable accuracy for a given integrated luminosity. Note that the assumed value for $\mathcal{L}$ is conservative; one expects in the best case to eventually obtain $\mathcal{L} = 160$ pb^{-1}/polarization at $\sqrt{S} = 200$ GeV and $\mathcal{L} = 400$ pb^{-1}/polarization at $\sqrt{S} = 500$ GeV. In any case, it is straightforward to rescale our predicted minimally observable asymmetry [2] if one prefers other values for $\mathcal{L}$, P or ϵ. We also emphasize that we have chosen rather small bins in $p_{T\gamma}$, $\Delta p_{T\gamma} = 2$ GeV. It would certainly seem advantageous in the actual data analysis to increase the bin size when going to larger $p_{T\gamma}$, as is indeed a commonly adopted procedure in the unpolarized prompt-photon experiments.

From fig. 6, we see that the shapes of the asymmetries obtained using the GRSV STD and GRSV MAXg sets are quite similar, but the difference in normalization is sizeable; this is

[2]Our cuts used in fig. 6, in particular $|\eta_\gamma| < 0.35$, actually correspond to those of the PHENIX experiment. Note, however, that all our results have been integrated over the full 2π of azimuthal angle, whereas the PHENIX electromagnetic calorimeter only covers half the azimuth. This implies that for a correct comparison our minimally observable asymmetry has to be multiplied by a factor of $\sqrt{2}$, in addition to introducing the appropriate values for $\mathcal{L}$, P, ϵ. Our results for $\left(\mathcal{A}_{p_{T\gamma}}\right)_{min}$ are then found to be consistent with those reported in [16].

consistent with what we observed in our study of jet physics [4]. On the other hand, the result obtained for GS-C looks completely different. At NLO, this asymmetry becomes negative in the region $10 < p_{T\gamma} < 30$ GeV at $\sqrt{S} = 200$ GeV, and in the region $30 < p_{T\gamma} < 45$ GeV at $\sqrt{S} = 500$ GeV. This is due in the first place to large cancellations between the contributions of various partonic channels: while the GRSV STD and GRSV MAXg results are dominated by the contribution of the qg-initiated subprocess, this is not true in the case of GS-C, where the gluon is so small that quark–quark scatterings (of opposite sign) are in absolute value of the same order or larger, in particular in the central pseudorapidity region, which is of interest here. For the same reason, the asymmetries for set GS-C obtained at the Born level turn out to be always substantially larger than those obtained at NLO. The issue of (non-)dominance of the qg subprocess, which is obviously of key interest for the extraction of the polarized gluon density from isolated-photon data, will be examined in more detail in the following.

It is instructive to compare the asymmetries at the two different centre-of-mass energies considered in fig. 6. As is well known, at smaller centre-of-mass energies, the asymmetries are generally larger; for example, when going from $\sqrt{S} = 200$ GeV to $\sqrt{S} = 500$ GeV the asymmetry obtained with GRSV STD decreases by a factor of about 3.6 (1.8) at $p_{T\gamma} = 10$ GeV ($p_{T\gamma} = 50$ GeV). This feature is readily explained by the fact that, for fixed $p_{T\gamma}$, at larger $\sqrt{S}$ one probes smaller values of x in the parton distributions. Since the unpolarized parton densities are steeper than the polarized ones towards small x's, one therefore gives more weight to the unpolarized cross section in the denominator of the asymmetry. However, when comparing the predicted asymmetries with the minimum observable asymmetry, it is clear that, at a fixed value of $p_{T\gamma}$, and except for the first few $p_{T\gamma}$ bins, the situation at $\sqrt{S} = 500$ GeV is more favourable than that at $\sqrt{S} = 200$ GeV. On the other hand, as far as a measurement of Δg at a given x is concerned, one should rather look at the asymmetries at fixed $x_T^\gamma = 2p_{T\gamma}/\sqrt{S}$, since this corresponds to the value at which the parton densities are probed predominantly. As can be seen from fig. 6, the asymmetries corresponding to the GRSV sets approximately scale with x_T^γ. Then, the quantity deciding about which energy is more favourable, is the minimally observable asymmetry at a given x_T^γ. This quantity does *not* scale with x_T^γ, as can be inferred from the figure. For $\sqrt{S} = 500$ GeV, one finds a value of $\left(\mathcal{A}_{p_{T\gamma}}\right)_{min}$ larger than for the lower energy, making the higher-energy option appear less favourable. However, two points should be kept in mind here: firstly, in both plots in fig. 6 the same value for the integrated luminosity has been used, whereas in reality one anticipates a higher (by a factor of 2 to 3) luminosity for $\sqrt{S} = 500$ GeV. Secondly, the *lower* cut-off for $p_{T\gamma}$ will certainly be the same for both energies, which means that at $\sqrt{S} = 500$ GeV one can explore a region of x_T^γ that is inaccessible at $\sqrt{S} = 200$ GeV. Also, even if one considers the same x_T^γ value for the two energies, the parton densities are still being probed at rather different scales, of the order of $x_T^\gamma\sqrt{S}/2$, the corresponding $p_{T\gamma}$ values. Thus, it will be interesting to see whether measurements performed at different centre-of-mass energies will yield information that is consistent, and compatible with QCD evolution.

The same asymmetries as presented in fig. 6 were also computed in a larger pseudorapidity range, $-1 < \eta_\gamma < 2$, relevant to the STAR experiment. In the case of the GRSV sets, only very minor differences were found, and the same conclusions as drawn above apply (we have also to take into account the fact that the minimally observable asymmetry decreases by a factor that can be as large as 2; therefore, in this larger pseudorapidity range the situation is

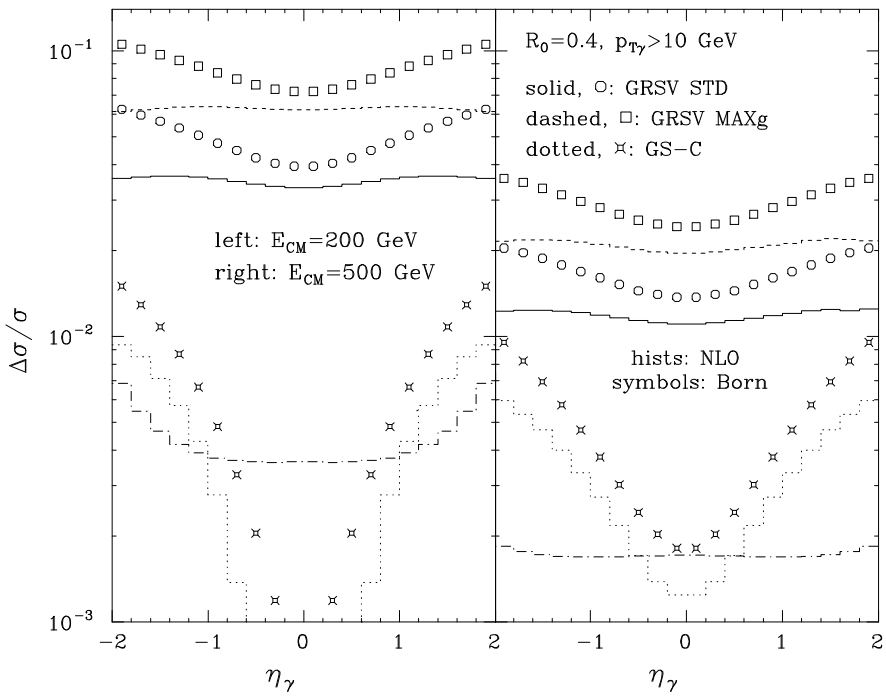

Figure 7: *As in fig. 6, but as a function of* η_γ.

even more favourable). In the case of GS-C, the asymmetry increases significantly, becoming larger than the minimally observable asymmetry for $p_{T\gamma} < 22$ GeV at $\sqrt{S} = 500$ GeV, and for $p_{T\gamma} < 14$ GeV at $\sqrt{S} = 200$ GeV. Also, in this region of $p_{T\gamma}$ the Born and NLO results are close to each other, displaying a behaviour similar to that of the GRSV sets. The reason is again linked to the dominance of the qg-initiated partonic subprocess: in fact, at large η_γ's, this subprocess accounts for most of the full NLO cross section also in the case of GS-C, as will be shown below. It thus follows that, if the true polarized gluon density is similar to the one of the GS-C set, an extended pseudorapidity coverage is mandatory in order to be able to see it experimentally. Finally, we mention that we computed the asymmetries also by varying the isolation parameters R_0 and n. When setting $R_0 = 0.7$ and/or $n = 2$, we did not find any noticeable difference with the results presented above.

In fig. 7 we present the asymmetry as a function of η_γ. A cut $p_{T\gamma} > 10$ GeV has been applied. We again show the results obtained at two different centre-of-mass energies, at both the Born and the NLO level. As in the case of the $p_{T\gamma}$ distribution, the shapes of the asymmetries obtained with the two GRSV sets are almost identical, while the one obtained with GS-C behaves quite differently. The NLO result for GS-C becomes negative around $\eta_\gamma = 0$ at $\sqrt{S} = 200$ GeV (the Born asymmetry remains positive), consistently with what we observed before in the low-$p_{T\gamma}$ region at this energy. As remarked before, away from the central-η_γ region the GS-C asymmetry is larger than the minimally observable one, and the Born and the NLO results become similar. On the other hand, in this region the Born and NLO results for the GRSV sets differ more than around $\eta_\gamma = 0$. This is simply related to the fact that here the polarized cross sections fall more rapidly at the NLO level than at the

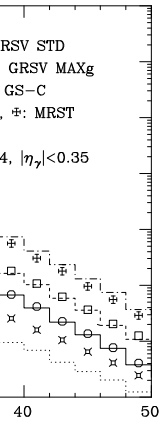

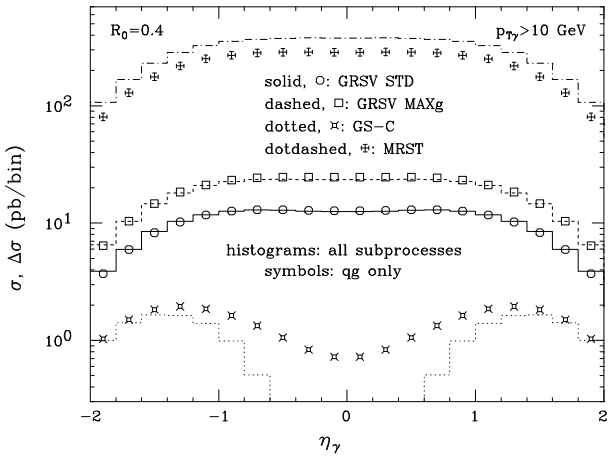

Figure 8: *$p_{T\gamma}$ and η_γ spectra of isolated photons in polarized and unpolarized collisions. The results obtained by retaining only the contribution of the qg-initiated partonic subprocess are also shown (symbols).*

Born level (cf. fig. 5), contrary to the case of the unpolarized cross section.

We now return to the issue of the dominance of the qg-initiated subprocess in prompt-photon production at RHIC. In fig. 8 we show the $p_{T\gamma}$ (left) and η_γ (right) dependences of the polarized and unpolarized cross sections, using the three sets of polarized parton densities employed in the previous figures. As before, the isolation of definition B and the default choice of scales have been adopted. We have used $\sqrt{S} = 200$ GeV here (we checked that at $\sqrt{S} = 500$ GeV we obtain results that lead us to the very same conclusions); cuts are as before. The symbols show in each case the cross section that is obtained by keeping only the qg-initiated subprocess. One can clearly see that in the polarized case, for the two GRSV density sets, the qg subprocess alone produces a result that is almost identical to the full answer. As we have checked, this comes about to some extent because the other subprocesses all give small contributions, but also because they tend to cancel one another to a good approximation. This explains why for set GS-C a different pattern is found: slightly different quark densities and a vastly different gluon distribution make the cancellation of the non-qg channels imperfect, and the gluon density is not large enough to render the signal from qg scattering dominant, except for large $|\eta_\gamma|$. However, in view of fig. 6, this finding does not really create a problem: if the gluon is indeed as small as embodied in the GS-C set, the measurement at RHIC will anyway only give an asymmetry compatible with zero, and we will not be in a position to actually unfold Δg from the data. If, on the other hand, Δg is sizeable, it is an encouraging result that the polarized cross section provides a very direct measure of it. Note that in the unpolarized case the qg channel is generally responsible for only $\mathcal{O}(80\%)$ of the cross section.

We finally mention that we have also computed the asymmetries by isolating the photon according to definition A. In the case of the GRSV sets, the results are almost identical to those shown here. In the case of GS-C, some difference can be seen in the central pseudorapidity region, where the asymmetry tends to be smaller in the case of definition A. Part of this effect

results from the different scale choices adopted for the two definitions, as discussed at the beginning of this section.

4 Isolated-photon-plus-jet observables

In the production process, the transverse momentum of the prompt photon is balanced by that of the high-p_T outgoing hadrons. It may be decided to neglect the properties of these hadrons, and to study the inclusive production of the photon, as we did in section 3. On the other hand, the study of the correlations between the photon and the associated hadrons gives a more thorough information on the underlying dynamics. Also, from the experimental point of view, photon-plus-hadron events can be used as a means of calibrating the hadronic calorimeter. In this section, we will consider photon-plus-jet observables. Our predictions are relevant to the STAR experiment [17] at RHIC, where one of the main goals is indeed to determine Δg from prompt-photon-plus-jet events. As is customary in any fixed-order computation in perturbative QCD, our predictions are given at the parton level (i.e. our jet-finding algorithm deals with partons and not with hadrons). We will adopt here a k_T-algorithm, namely that proposed in ref. [44], with $D = 1$. We will only discuss the case when the photon is isolated following the prescription B; unless otherwise specified, we will adopt the isolation parameters given in eq. (8): $R_0 = 0.4$, $\epsilon_\gamma = 1$, $n = 1$. Since our computation is based on five-leg amplitudes, we are able to predict the photon-plus-one-jet observables at NLO, and the photon-plus-two-jet observables at LO.

4.1 General features and perturbative stability

The number of jets that accompany the photon does depend not only upon the dynamics, but also upon the jet-finding algorithm and the kinematical cuts imposed on the jets. This is documented in table 1, where the total rates are presented for events satisfying

$$p_{T\gamma} \geq 10 \text{ GeV}, \quad -1 \leq \eta_\gamma \leq 2, \qquad p_{Tj} \geq 10, 12, 14 \text{ GeV}, \quad -1 \leq \eta_j \leq 2, \tag{11}$$

in the case of polarized and unpolarized pp collisions at $\sqrt{S} = 500$ GeV (p_{Tj} and η_j are the jet transverse momentum and pseudorapidity, respectively). The cuts on η_γ, η_j considered here are relevant to the STAR detector. As one might expect, there is only a small fraction of events where the photon is accompanied by two jets (in the case of two-jet events, the transverse-momentum cut is applied to both jets; it is clear that the inclusion of radiative corrections for photon-plus-two-jet observables will not change what was said before). On the other hand[3], a sizeable number of events falls in the class denoted by '0-jets', which is constituted by those events where the jet(s) do not pass the imposed transverse-momentum or pseudorapidity cuts; at the lowest transverse-momentum cut, this is mainly due to the fact that the pseudorapidity cut is not symmetric around $\eta = 0$. Since the number of jets is directly related to the hardness of the event, large differences can be seen in the ratio of two-jet over one-jet rates, when different parton densities are considered. In particular, this

[3]By definition, for a given row in table 1, the sum '0-jet'+'1-jet'+'2-jet' is the same for each of the three p_{Tj} cuts, and corresponds to the inclusive isolated-photon rate.

	$p_{Tj} \geq 10$ GeV			$p_{Tj} \geq 12$ GeV			$p_{Tj} \geq 14$ GeV		
	0-jet	1-jet	2-jet	0-jet	1-jet	2-jet	0-jet	1-jet	2-jet
GRSV STD	115.1	168.0	15.87	136.7	151.4	10.92	178.0	113.3	7.692
GRSV MAXg	206.7	294.7	29.28	244.6	265.8	20.30	317.2	199.1	14.41
GS-C	27.73	41.57	1.121	37.30	32.52	0.604	49.61	20.50	0.312
MRST$\cdot 10^{-3}$	11.61	13.27	0.730	14.37	10.77	0.471	18.45	6.854	0.310

Table 1: *Total rates (in pb; the entries relevant to unpolarized scattering have been multiplied by* 10^{-3}*) for isolated-photon-plus-jet events, at* $\sqrt{S} = 500$ *GeV.*

ratio is the larger the slower the gluon density approaches zero for $x \to 1$; while GRSV STD and GRSV MAXg return almost the same ratio (the shape of their gluon being basically the same), the result for GS-C is much smaller, since the gluon density in this case has a dip at intermediate x values. It follows that a first rough piece of information on the behaviour of the gluon density at large x can be obtained by simply looking at the *total* photon-plus-jet rates. We also notice that the result for the ratio of one-jet over two-jet rates in the case of unpolarized scattering (fourth row in table 1) lies in between that of the GRSV sets and that of the GS-C set, consistently with the fact that the shape of the MRST gluon density is softer than that of GRSV STD and harder than that of GS-C. This also implies that the ratio of rates corresponding to different numbers of jets is not very sensitive to the polarization of the beams.

We must stress that, in the case of $p_{Tj} \geq 10$ GeV *and* $p_{T\gamma} \geq 10$ GeV, the zero-jet and one-jet rates are rather pathological in perturbative QCD (on the other hand, their sum is well-behaved). Indeed, when equal transverse-momentum cuts are imposed on the photon and the hardest jet, large logarithms appear in the cross section, which in principle should be resummed. Roughly speaking, at any fixed order in perturbation theory, for 'symmetric cuts' the radiation of real gluons cannot compensate the large and negative contribution of the virtual diagrams. The mechanism is identical to the one that can be observed in two-jet correlations, in the case when the two jets have the same minimum transverse momentum cut. This matter was discussed at length in ref. [45], to which we refer the reader for more details. For illustration, we consider here the total rate (no η cuts have been applied; these would just change the absolute normalization which is of no interest in what follows):

$$\sigma_{\gamma j}(\Delta) = \sigma(p_{T\gamma} \geq 10 \text{ GeV}, p_{Tj} \geq 10 \text{ GeV} + \Delta) \tag{12}$$

as a function of Δ, for both polarized and unpolarized collisions, at different centre-of-mass energies. By definition, the jet is the hardest of the jets of the event. The results are displayed in fig. 9. The plots in this figure are completely analogous to the ones in fig. 4 of ref. [45]. The main point is that a negative slope is here visible at $\Delta = 0$, implying that the cross section *decreases* here with the *decreasing* cut on $p_{T\gamma}$, clearly signalling a failure of the perturbative expansion. We remark, however, that, at variance with the case of jet–jet correlations, in the case of isolated-photon-plus-jet production, a value of $\Delta = 1$ GeV already appears to be perfectly safe. We also remind the reader that, even in the case of equal transverse-

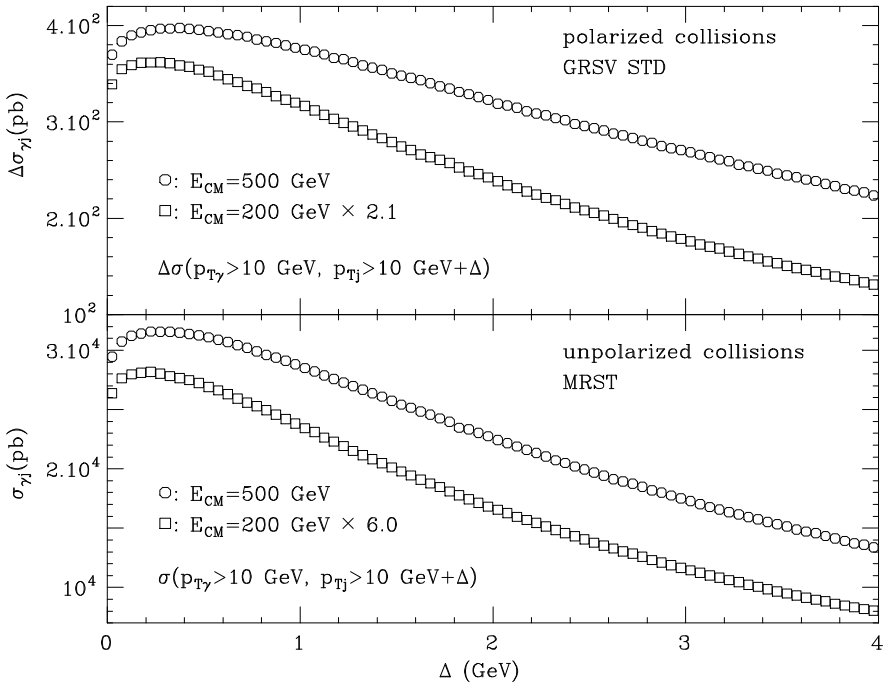

Figure 9: *Total photon-plus-jet rates, in polarized and unpolarized collisions, at different centre-of-mass energies.*

momentum cuts, the perturbative expansion is reliable everywhere except in some corners of the phase space (examples will be given below). Inspecting fig. 9, we finally note that, when going from $\sqrt{S} = 200$ GeV to $\sqrt{S} = 500$ GeV, the cross section increases much more in the unpolarized than in the polarized case. This implies that, as in the case of inclusive observables discussed in the previous section, at fixed final-state kinematical variables the asymmetries for photon-plus-jet observables are larger at the smaller centre-of-mass energies.

We now turn to the issue of the perturbative stability of our results for correlations between photon and jets. Since we are interested in NLO predictions, we will only consider photon-plus-one-jet quantities; in the case when two jets are present in the event, only the hardest jet is retained. As in subsection 3.1, we will assume that we obtain a (relatively sound) indication of the stability of the cross sections if the variations induced by changing the renormalization and factorization scales with respect to their default values are small. In fig. 10 we present the result for the invariant mass distribution of the photon-jet system, in the case of polarized collisions at $\sqrt{S} = 500$ GeV. The pseudorapidities of both the photon and the jet are required to be in the range $-1 \leq \eta \leq 2$, and we impose $p_{T\gamma} \geq 10$ GeV and $p_{Tj} \geq 10$ GeV. The results of both the NLO computation (upper curves) and Born computation (lower curves, which have been rescaled in order to make them clearly distinguishable from the NLO ones) are displayed. Similarly to the case of the inclusive transverse momentum distribution of isolated photons (cf. fig. 1), in most of the range in $M_{\gamma j}$ the change of cross section induced by a variation of the renormalization scale is of the order of 10% at NLO, and larger at the Born level. However, a quite dramatic effect is seen at threshold, when radiative corrections are

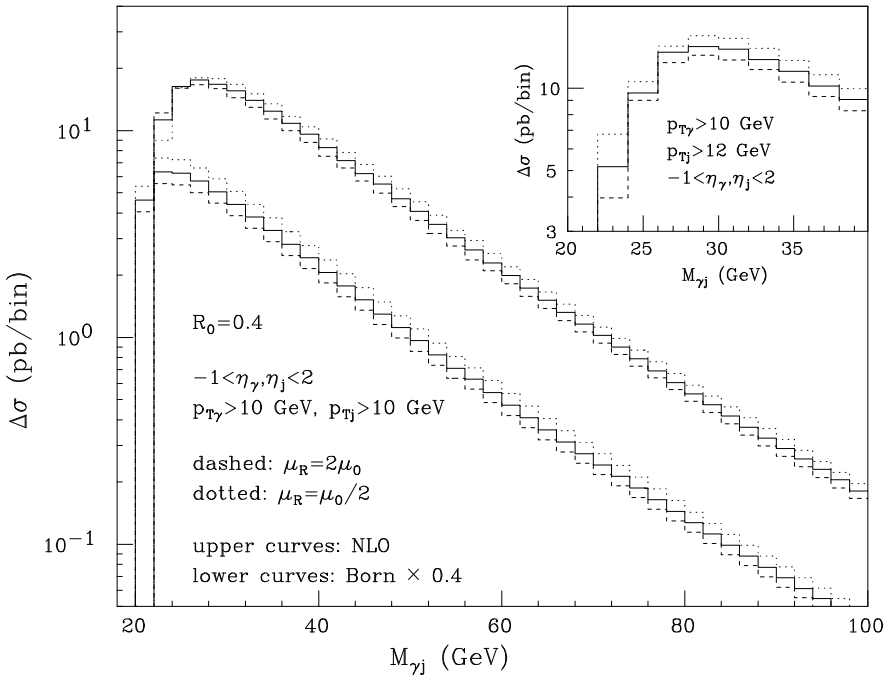

Figure 10: *Renormalization-scale dependence of the invariant mass spectrum of the photon–jet system, at the Born and NLO levels. The result for unequal lower transverse-momentum cuts is also shown (inset).*

included: the cross section in the first bin becomes negative, and the scale dependence displays a pathological behaviour in this range, the cross section becoming smaller for decreasing renormalization scales. This effect is exactly a consequence of the fact that the minimum transverse-momentum cuts on the photon and the jet are equal. Indeed, in the inset of fig. 10 we show (in the threshold region) the invariant mass of the photon–jet system in the case when $p_{Tj} \geq 12$ GeV. It is obvious that here the scale dependence is as expected, and the cross section in the first bin (although not visible in the figure) remains positive. However, the first two bins show a scale sensitivity comparable to the one of the Born result. In fact, close to the threshold the NLO result is effectively a LO one, since the threshold at the Born level is in this case at $M_{\gamma j} = 24$ GeV. In the invariant mass range not close to threshold, the scale dependence in the case of unequal transverse-momentum cuts is practically identical to the one displayed in the main body of fig. 10. We also studied the factorization scale dependence of the invariant mass distribution. In the region not close to the threshold, there is a clear improvement when going from LO to NLO; again, the results for equal and unequal transverse-momentum cuts are very similar. At threshold, the same considerations as given above apply. As in the case of the single-inclusive photon transverse-momentum spectrum displayed in fig. 1, the cross section for larger (smaller) factorization scales is larger (smaller) than the default one at small invariant masses, while it is smaller (larger) than the default for large invariant masses. This behaviour is almost entirely due to scale dependence of the parton densities, as already discussed in the single-inclusive case.

We performed a thorough study of the renormalization and factorization scale dependence

of many photon-jet observables. In particular, we considered the photon (jet) transverse momentum and pseudorapidity distributions, when cuts on the recoiling jet (photon) are imposed, as suggested in ref. [26]. Among the photon-jet correlations, we considered the transverse momentum of the pair $p_T^{(\gamma j)}$, the azimuthal distance in the transverse plane $\Delta\phi_{\gamma j}$, the distance in the η–ϕ plane $\Delta R_{\gamma j}$, and the variables

$$x_1 = \frac{p_{T\gamma} e^{\eta_\gamma} + p_{Tj} e^{\eta_j}}{\sqrt{S}}, \qquad x_2 = \frac{p_{T\gamma} e^{-\eta_\gamma} + p_{Tj} e^{-\eta_j}}{\sqrt{S}}, \tag{13}$$

which, at the Born level, coincide with the Bjørken-x values of the incoming partons. In all these cases, a reduction in the relative size of the scale dependence is seen at the NLO with respect to the Born level, whenever such a comparison is meaningful (that is whenever the Born contribution is already present at the level of a $2 \to 2$ scattering process): a change of the scales within the limits as above induces a variation of the results of about 10% or less. In the regions of the phase space where the partonic contributions start at the $2 \to 3$ level (for example, $p_T^{(\gamma j)} > 0$, $\Delta\phi_{\gamma j} < \pi$, $\Delta R_{\gamma j} < \pi$), our NLO results have a scale dependence larger than elsewhere, of the order of 15% to 20%, since they are effectively LO. Finally, as in the case of the invariant-mass distribution, there are corners of the phase space where the perturbative results are not reliable in the case of equal transverse-momentum cuts. Among those, the case of $\Delta R_{\gamma j} = \pi$ is particularly interesting, since here the Born threshold falls inside the range available at NLO. This case has been described, on general grounds, in ref. [46].

4.2 Spin asymmetries

We now turn to the study of asymmetries for photon-plus-jet cross sections. We follow the procedure of subsection 3.2, namely we study the dependence of the asymmetries on the choice of polarized parton densities, at the Born and NLO levels. Here, we restrict ourselves to $\sqrt{S} = 200$ GeV. We verified that the pattern when going to $\sqrt{S} = 500$ GeV is similar to the one already described in the preceding section; namely, at fixed final-state kinematics we get smaller asymmetries, with however also smaller minimally observable asymmetries. In fig. 11 we show the asymmetries as functions of the invariant mass (left) and x_1 (right). The photon-plus-jet events have been selected by imposing equal transverse-momentum cuts on the photon and on the hardest jet ($p_T > 10$ GeV; pseudorapidities are restricted to the range $-1 < \eta < 2$). As discussed previously, this choice only affects the threshold region of the invariant mass, where our predictions should not be considered as reliable. As in the case of single-inclusive quantities, the results for GRSV STD and GRSV MAXg are pretty similar in shape, although sizeably different in normalization. On the other hand, GS-C has a clearly distinguishable signature, showing a dip at intermediate values of the invariant mass and in the region around $x_1 = 0.1$. It is very easy to trace the origin of this behaviour back to the shape of the GS-C gluon. The NLO results are smaller than those at LO, as they already were in the case of inclusive observables. The difference between Born and NLO results is not big at small invariant masses and in the whole x_1 range, while it grows larger in the tail of the invariant-mass distribution, since the K-factor of the unpolarized cross section is larger in this region than that of the polarized cross section. Figure. 11 also presents the minimally observable asymmetry (dot-dashed histograms), calculated according to eq. (10). A bin size

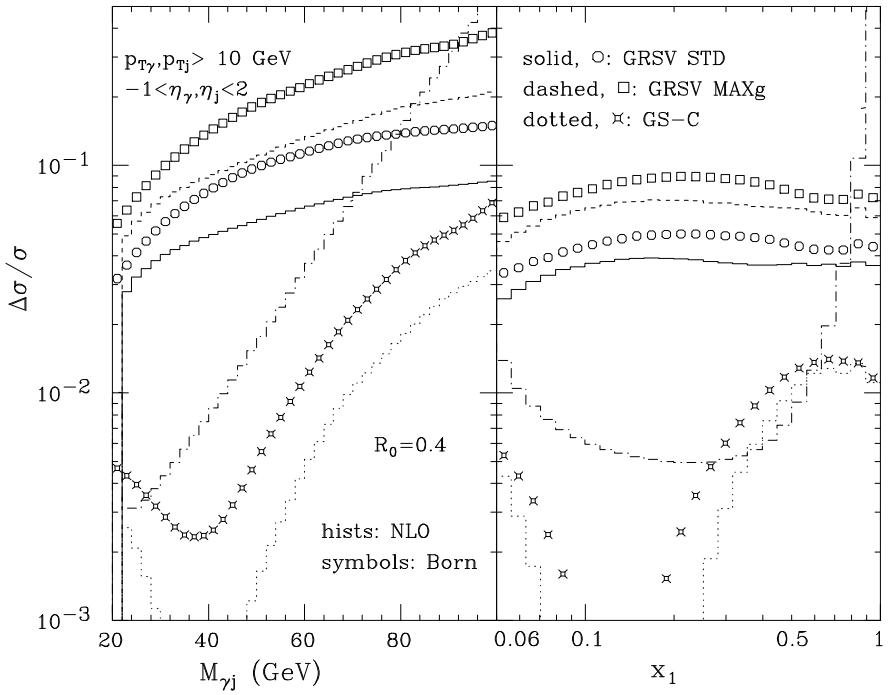

Figure 11: *Asymmetries at $\sqrt{S} = 200$ GeV, as functions of invariant mass (left) and x_1 (right). The NLO (histograms) and Born (symbols) results are both shown. The minimum observable asymmetry is displayed by the dot-dashed histogram.*

of 2 GeV has been chosen for $M_{\gamma j}$, and of 0.05 for $\log x_1$; as before, $\mathcal{L} = 100$ pb^{-1} and $\epsilon = P = 1$. It is apparent that, if the polarized densities are as predicted by the GS-C set, the measurement of the asymmetry at RHIC will produce a result compatible with zero, even if quite large integrated luminosities are attained. This result is consistent with what we already found in section 3.2; however, in the case of single-inclusive variables the situation appeared to be slightly better, when the enlarged pseudorapidity range $-1 < \eta < 2$ was considered.

In this context, we would like to comment on the findings of ref. [26], where it was observed that, by looking at photon-plus-jet events, instead of considering only the inclusive variables of the photon, one gets larger asymmetries. Also, photon-plus-jet observables enhance the sensitivity to the shape of the parton densities and can be used for a more straightforward deconvolution of Δg from data [17]. Although we agree with these observations, we doubt that photon-plus-jet correlations will give us a better chance of measuring the gluon density than inclusive observables. In fact, there is in practice the problem that the (theoretical) minimally observable asymmetry is larger in the case of photon-plus-jet quantities than in the case of inclusive-photon quantities. The situation is summarized in fig. 12, for the case of the η_γ spectrum with $p_{T\gamma} \geq 10$ GeV. In the case of the photon-plus-jet observable, the following cuts have been imposed on the jet: $p_{Tj} \geq 10$ GeV, $|\eta_j| \leq 0.5$. From the figure, it is apparent that, in spite of the fact that the asymmetry is increased when cutting on the jet variables, the measurement would be more difficult, since the minimally observable asymmetry is enhanced by a larger factor with respect to the asymmetry. Of course, this is

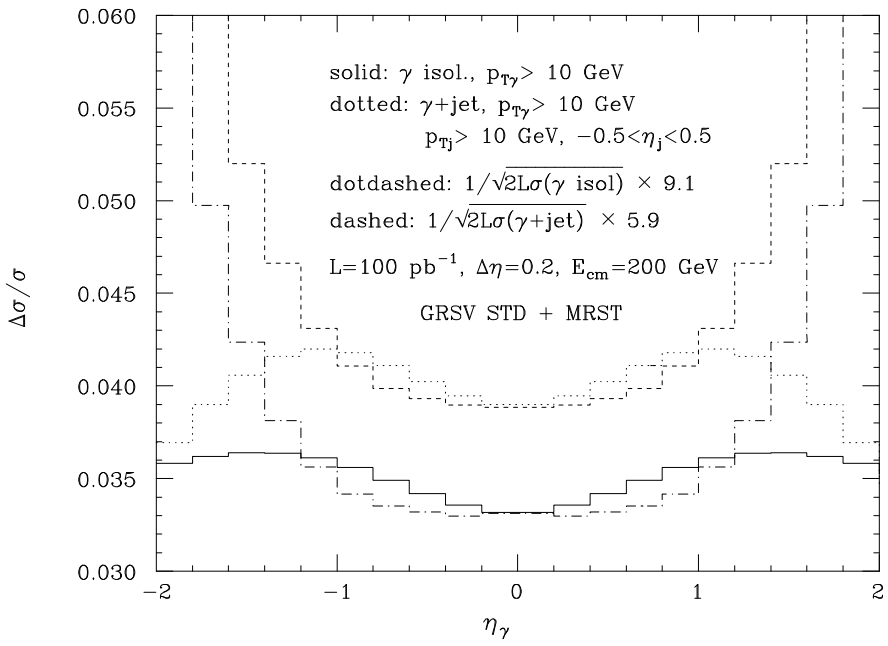

Figure 12: *Asymmetries at $\sqrt{S} = 200$ GeV, as functions of photon pseudorapidity, with (dotted) and without (solid) a transverse-momentum cut on the recoiling jet. The corresponding minimally observable asymmetries (dashed and dot-dashed, respectively) have been rescaled in order to coincide with the respective asymmetries at $\eta_\gamma = 0$.*

a purely theoretical estimate, which assumes that the experimental efficiency is the same in the case of inclusive-photon or photon-plus-jet events (here taken to be equal to 1). This is probably unrealistic, but it seems unlikely that the photon-plus-jet efficiency will be higher than that for photon-tagging only. Therefore, without any detailed study at the detector level, it seems improbable that the photon-plus-jet asymmetries will be the preferred tool for pinning down the polarized gluon density. We finally also have to add that in ref. [26] the photon transverse momentum was constrained in a bin around $p_{Tj} = 10$ GeV of width 1 GeV, instead of having $p_{T\gamma} > 10$ GeV as in fig. 12. In view of the discussion relative to fig. 9, the kinematical constraints imposed in ref. [26] appear to be more problematic from the perturbative point of view than those adopted in this paper for producing fig. 12.

5 Conclusions

We have performed a phenomenological study of prompt-photon production by polarized colliding proton beams at RHIC. Our main motivation has been to put in practice a recently proposed alternative way of isolating the photon from the hadronic background, which eliminates the ill-understood fragmentation contribution from the cross section, so that only the direct component is left. In this way, an optimally clean photon signal results. This has also enabled us to perform the first fully consistent next-to-leading order calculation for polarized

prompt-photon production.

We have compared the cross sections and asymmetries for the new isolation with those obtained for a traditional cone-type isolation as used hitherto in unpolarized collider prompt-photon experiments. We find only small differences, implying that using the new 'clean' isolation is not accompanied by a reduction in the number of events.

Performing a consistent next-to-leading order study, we were in a position to examine the perturbative stability of the cross sections by studying their dependence on the factorization and renormalization scales. We find that the scale dependence is significantly reduced when going from the Born level to the next-to-leading order, and that the scale dependence is moderate at next-to-leading order. This generally holds true for both inclusive isolated-photon production and for isolated-photon-plus-jet production.

We have presented phenomenological results for the spin asymmetries and their expected statistical errors in the RHIC experiments PHENIX and STAR. Consistently with previous studies, the results are highly sensitive to the size of the spin-dependent gluon density $\Delta g(x, Q^2)$, and it turns out that, unless Δg is very small, it should clearly be possible to rather accurately determine it in the region $0.04 < x < 0.25$, at scales of the order of the transverse momentum of the photon, 10 GeV $< p_{T\gamma} <$ 30 GeV. In this context, we find that as far as statistics is concerned, inclusive-photon measurements seem to be somewhat more favourable than photon-plus-jet ones.

Acknowledgements

We are happy to thank G. Ridolfi for his collaboration at an early stage of this work. We are also grateful to N. Saito for useful information. The work of S.F. is supported in part by the EU Fourth Framework Programme 'Training and Mobility of Researchers', Network 'Quantum Chromodynamics and the Deep Structure of Elementary Particles', contract FMRX-CT98-0194 (DG 12 - MIHT).

References

[1] I. Bojak and M. Stratmann, *Nucl. Phys.* **B540** (1999) 345; *Phys. Lett.* **B433** (1998) 411.

[2] G. Baum et al., COMPASS collab., CERN/SPSLC 96-14.

[3] S. Frixione and G. Ridolfi, *Phys. Lett.* **B383** (1996) 227;
M. Stratmann and W. Vogelsang, *Z. Phys.* **C74** (1997) 641; Proc. of the 1995/96 workshop on 'Future Physics at HERA', Hamburg, Germany, eds. G. Ingelman, A. De Roeck, and R. Klanner, p. 815.

[4] D. de Florian, S. Frixione, A. Signer and W. Vogelsang, *Nucl. Phys.* **B539** (1999) 455.

[5] D. de Florian and S. Frixione, *Phys. Lett.* **B457** (1999) 236.

[6] RHIC Spin Collab., D. Hill et al., letter of intent RHIC-SPIN-LOI-1991, updated 1993;
G. Bunce et al., *Particle World* **3** (1992) 1.

[7] For a compilation of the prompt-photon data in the unpolarized case, see: W. Vogelsang and M. Whalley, *J. Phys.* **G23** (1997) A1.

[8] D. Buskulic et al., ALEPH Collab., *Z. Phys.* **C69** (1996) 365;
K. Ackerstaff et al., OPAL Collab., *Eur. Phys. J.* **C2** (1998) 39.

[9] P. Aurenche, P. Chiappetta, M. Fontannaz, J.Ph. Guillet and E. Pilon, *Nucl. Phys.* **B399** (1993) 34.

[10] M. Glück, L.E. Gordon, E. Reya and W. Vogelsang, *Phys. Rev. Lett.* **73** (1994) 388.

[11] W. Vogelsang and A. Vogt, *Nucl. Phys.* **B453** (1995) 334.

[12] P. Aurenche, M. Fontannaz, J.Ph. Guillet, B. Kniehl, E. Pilon and M. Werlen, *Eur. Phys. J.* **C9** (1999) 107.

[13] M. Glück, E. Reya, and A. Vogt, *Phys. Rev.* **D48** (1993) 116; E: **D51** (1995) 1427.

[14] L. Bourhis, M. Fontannaz and J.Ph. Guillet, *Eur. Phys. J.* **C2** (1998) 529.

[15] E.L. Berger and J. Qiu, *Phys. Rev.* **D44** (1991) 2002.

[16] Y. Goto, talk given at the '7th International Workshop on Deep Inelastic Scattering and QCD (DIS 99)', Zeuthen, Germany, April 1999;
Y. Goto, N. Hayashi and N. Saito, *Background Study for Prompt Photon Production at PHENIX* (internal RIKEN report).

[17] L.C. Bland, `hep-ex/9907058`, to be published in the proceedings of 'Workshop on Physics with Electron Polarized Ion Collider - EPIC '99', Bloomington, Indiana, April 1999.

[18] S. Güllenstern, P. Gornicki, L. Mankiewicz and A. Schäfer, *Phys. Rev.* **D51** (1995) 3305;
G.P. Skoro, M. Zupan and M.V. Tokarev, `hep-ph/9905511`.

[19] N. Mobed, C. Papavasiliou and M. Svec, *Phys. Rev.* **D26** (1982) 3284;
E.L. Berger and J. Qiu, *Phys. Rev.* **D40** (1989) 778;
S. Gupta, D. Indumathi and M. Murthy, *Z. Phys.* **C42** (1989) 493; E: **C44** (1989) 356;
H.-Y. Cheng and S.-N. Lai, *Phys. Rev.* **D41** (1990) 91;
C. Bourrely, J.Ph. Guillet and J. Soffer, *Nucl. Phys.* **B361** (1991) 72;
P. Mathews and R. Ramachandran, *Z. Phys.* **C53** (1992) 305;
P. Chiappetta, P. Colangelo, J.Ph. Guillet and G. Nardulli, *Z. Phys.* **C59** (1993) 629.

[20] A.P. Contogouris, B. Kamal, Z. Merebashvili and F.V. Tkachov, *Phys. Lett.* **B304** (1993) 329; *Phys. Rev.* **D48** (1993) 4092.

[21] L.E. Gordon and W. Vogelsang, *Phys. Rev.* **D48** (1993) 3136.

[22] A.P. Contogouris and Z. Merebashvili, *Phys. Rev.* **D55** (1997) 2718.

[23] L.E. Gordon and W. Vogelsang, *Phys. Rev.* **D49** (1994) 170.

[24] L.E. Gordon and W. Vogelsang, *Phys. Rev.* **D50** (1994) 1901.

[25] L.E. Gordon, *Nucl. Phys.* **B501** (1997) 197;
L.E. Gordon and G.P. Ramsey, *Phys. Rev.* **D59** (1999) 074018.

[26] S. Chang, C. Coriano and L.E. Gordon, *Phys. Rev.* **D58** (1998) 074002.

[27] S. Frixione, *Phys. Lett.* **B429** (1998) 369.

[28] F. Abe et al., CDF Collab., *Phys. Rev. Lett.* **73** (1994) 2662; E: **74** (1995) 1891;
S. Kuhlmann, CDF Collab., FERMILAB-CONF-99-165-E;
L. Apanasevich et al., E706 Collab., *Phys. Rev. Lett.* **81** (1998) 2642;
G. Ballocchi et al., UA6 Collab., *Phys. Lett.* **B436** (1998) 222.

[29] J. Huston et al., *Phys. Rev.* **D51** (1995) 6139;
H. Baer and M. Hall Reno, *Phys. Rev.* **D54** (1996) 2017;
L. Apanasevich et al., *Phys. Rev.* **D59** (1999) 074007.

[30] A.D. Martin, R.G. Roberts, W.J. Stirling and R.S. Thorne, *Eur. Phys. J.* **C4** (1998) 463.

[31] H.-L. Lai and H. Li, *Phys. Rev.* **D58** (1998) 114020.

[32] E. Laenen, G. Oderda and G. Sterman, *Phys. Lett.* **B438** (1998) 173;
S. Catani, M.L. Mangano and P. Nason, *JHEP* **9807** (1998) 024.

[33] S. Catani, M.L. Mangano, P. Nason, C. Oleari and W. Vogelsang,
JHEP **9903** (1999) 025.

[34] H. Baer, J. Ohnemus and J. F. Owens, *Phys. Rev.* **D42** (1990) 61;
P. Aurenche, R. Baier and M. Fontannaz, *Phys. Rev.* **D42** (1990) 1440;
E. W. N. Glover and W. J. Stirling, *Phys. Lett.* **B295** (1992) 128;
Z. Kunszt and Z. Trocsanyi, *Nucl. Phys.* **B394** (1993) 139.

[35] S. Catani, M. Fontannaz and E. Pilon, *Phys. Rev.* **D58** (1998) 094025.

[36] E. W. N. Glover and A. G. Morgan, *Z. Phys.* **C62** (1994) 311;
A. Gehrmann-De Ridder and E. W. N. Glover, *Nucl. Phys.* **B517** (1998) 269.

[37] F. Aversa, P. Chiappetta, M. Greco and J.Ph. Guillet, *Phys. Lett.* **B211** (1988) 465;
Nucl. Phys. **B327** (1989) 105.

[38] S. Frixione, Z. Kunszt and A. Signer, *Nucl. Phys.* **B467** (1996) 399.

[39] S. Frixione, *Nucl. Phys.* **B507** (1997) 295.

[40] S. Frixione, `hep-ph/9809397`, Proc. of the '29th International Conference on High-Energy Physics (ICHEP 98)', Vancouver, Canada, July 1998.

[41] M. Glück, E. Reya, M. Stratmann and W. Vogelsang, *Phys. Rev.* **D53** (1996) 4775.

[42] Particle Data Group, C. Caso et al., *Eur. Phys. J.* **C3** (1998) 1.

[43] T. Gehrmann and W.J. Stirling, *Phys. Rev.* **D53** (1996) 6100.

[44] S.D. Ellis and D. Soper, *Phys. Rev.* **D48** (1993) 3160.

[45] S. Frixione and G. Ridolfi, *Nucl. Phys.* **B507** (1997) 315.

[46] S. Catani and B.R Webber, *JHEP* **9710** (1997) 005.